Sea Surface Temperature Sensitivity to Water Turbidity from Simulations of the Turbid Black Sea Using HYCOM*

A. BIROL KARA, ALAN J. WALLCRAFT, AND HARLEY E. HURLBURT

Oceanography Division, Naval Research Laboratory, Stennis Space Center, Mississippi

(Manuscript received 1 August 2003, in final form 15 April 2004)

ABSTRACT

This paper examines the sensitivity of sea surface temperature (SST) to water turbidity in the Black Sea using the eddy-resolving (~3.2-km resolution) Hybrid Coordinate Ocean Model (HYCOM), which includes a nonslab *K*-profile parameterization (KPP) mixed layer model. The KPP model uses a diffusive attenuation coefficient of photosynthetically active radiation (k_{PAR}) processed from a remotely sensed dataset to take water turbidity into account. Six model experiments (expt) are performed with no assimilation of any ocean data and wind/thermal forcing from two sources: 1) European Centre for Medium-Range Weather Forecasts (ECMWF) reanalysis (ERA) and 2) Fleet Numerical Meteorology and Oceanography Center (FNMOC) Navy Operational Global Atmospheric Prediction System (NOGAPS). Forced with ECMWF, experiment 1 uses spatially and monthly varying k_{PAR} values over the Black Sea, experiment 2 assumes all of the solar radiation is absorbed at the sea surface, and experiment 3 uses a constant k_{PAR} value of 0.06 m^{-1}, representing clear-water constant solar attenuation depth of 16.7 m. Experiments 4, 5, and 6 are twins of 1, 2, and 3 but forced with NOGAPS. The monthly averaged model SSTs resulting from all experiments are then compared with a fine-resolution (~9 km) satellite-based monthly SST climatology (the Pathfinder climatology). Because of the high turbidity in the Black Sea, it is found that a clear-water constant attenuation depth (i.e., expts 3 and 6) results in SST bias as large as 3°C in comparison with standard simulations (expts 1 and 4) over most of the Black Sea in summer. In particular, when using the clear-water constant attenuation depth as opposed to using spatial and temporal k_{PAR}, basin-averaged rms SST difference with respect to the Pathfinder SST climatology increases ~46% (from 1.41°C in expt 1 to 2.06°C in expt 3) in the ECMWF forcing case. Similarly, basin-averaged rms SST difference increases ~36% (from 1.39°C in expt 4 to 1.89°C in expt 6) in the NOGAPS forcing case. The standard HYCOM simulations (expts 1 and 4) have a very high basin-averaged skill score of 0.95, showing overall model success in predicting climatological SST, even with no assimilation of any SST data. In general, the use of spatially and temporally varying turbidity fields is necessary for the Black Sea OGCM studies because there is strong seasonal cycle and large spatial variation in the solar attenuation coefficient, and an additional simulation using a constant k_{PAR} value of 0.19 m^{-1}, the Sea-Viewing Wide Field-of-View Sensor (SeaWiFS) space–time mean for the Black Sea, did not yield as accurate SST results as experiments 1 and 4. Model–data comparisons also revealed that relatively large HYCOM SST errors close to the coastal boundaries can be attributed to the misrepresentation of land–sea mask in the ECMWF and NOGAPS products. With the relatively accurate mask used in NOGAPS, HYCOM demonstrated the ability to simulate accurate SSTs in shallow water over the broad northwest shelf in the Black Sea, a region of large errors using the inaccurate mask in ECMWF. A linear relationship is found between changes in SST and changes in heat flux below the mixed layer. Specifically, a change of ~50 W m^{-2} in submixed-layer heat flux results in a SST change of ~3.0°C, a value that occurs when using clear-water constant attenuation depth rather than monthly varying k_{PAR} in the model simulations, clearly demonstrating potential impact of penetrating solar radiation on SST simulations.

1. Introduction and motivation

The Black Sea is nearly landlocked, except for a narrow opening to the Bosporus Strait, resulting in poor ventilation of the deep waters by lateral fluxes (e.g., Sur et al. 1996). Extensive biological activity in the Black Sea is evident from various studies (e.g., Konovalov and Murray 2001; Oguz et al. 2001, 2002). The Black Sea also experiences large volumes of nutrients and contaminants from the Danube, Dniepr, and Dniestr Rivers along the northwestern shelf (e.g., Mee 1992; Guieu and Martin 2002; Wijsman et al. 2002). Permanent high turbidity due to the biological activities and river sources exists in the region because strong density stratification effectively inhibits vertical mixing and ventilation of subpycnocline waters from the surface. Thus, prediction of upper-ocean quantities in the region is closely tied to water turbidity in modeling studies.

* Naval Research Laboratory Contribution Number NRL/JA/7320/03/0019.

Corresponding author address: Birol Kara, Naval Research Laboratory, Code 7320, Bldg. 1009, Stennis Space Center, MS 39529-5004.
E-mail: kara@nrlssc.navy.mil

TABLE 1. The eddy-resolving ocean models commonly used in previous Black Sea studies: POM, MOM, DieCAST, and GHER. The numerical ocean model used in each study is given, along with its approximate grid resolutions in latitude and longitude (lat × lon) and the number of layers/levels in the vertical direction. Zonal grid spacing (km) is calculated using $\Delta x = 111.2 \times \cos(43^\circ) \times \Delta\text{lon}$, where $1^\circ \approx 111.2$ km and the central latitude is taken as 43° in the Black Sea. Meridional grid spacing (km) is calculated using $\Delta y = 111.2 \times \Delta\text{lat}$. HYCOM uses a $\frac{1}{25}^\circ$ Mercator grid, which is square (i.e., $\Delta x = \Delta y$) everywhere.

Black Sea eddy-resolving numerical modeling studies	OGCM used	OGCM grid resolution		Layers in vertical direction
		lat × lon (°)	$\Delta x \times \Delta y$ (km)	
Oguz et al. (1995)	POM	1/10° × 1/10°	08.5 × 11.5	18
Stanev et al. (1995)	MOM	1/4° × 1/3°	27.0 × 28.0	11
Oguz and Malanotte-Rizzoli (1996)	POM	1/10° × 1/10°	08.5 × 11.5	18
Rachev and Stanev (1997)	MOM	1/10° × 1/6°	14.0 × 11.0	22
Staneva and Stanev (1998)	MOM	1/4° × 1/3°	27.0 × 28.0	24
Staneva et al. (1999)	MOM	1/4° × 1/3°	27.0 × 28.0	24
Stanev and Rachev (1999)	MOM	1/10° × 1/6°	14.0 × 11.0	06
Stanev and Beckers (1999)	GHER	1/8° × 1/6°	15.0 × 15.0	25
Stanev and Staneva (2000)	MOM	1/12° × 1/9°	09.0 × 09.0	24
Kourafalou and Stanev (2001)	POM	1/12° × 1/9°	09.0 × 09.0	16
Grégoire and Lacroix (2001)	GHER	1/25° × 1/17°	05.0 × 05.0	25
Stanev and Staneva (2001)	MOM	1/12° × 1/9°	09.0 × 09.0	24
Staneva et al. (2001)	DieCAST	1/12° × 1/9°	09.0 × 09.0	20
Beckers et al. (2002)	GHER	1/8° × 1/6°	15.0 × 15.0	25
Beckers et al. (2002)	GHER	1/25° × 1/17°	05.0 × 05.0	25
This study	HYCOM	1/32° × 1/25°	03.2 × 03.2	15

Ocean general circulation models (OGCMs) with mixed layer submodels are necessary to explain air–sea interactions and upper ocean characteristics, such as sea surface temperature (SST). Prediction of SST on a wide variety of temporal and spatial scales is the focus of this paper. Realistic SST predictions from OGCMs are particularly needed over the biologically active Black Sea. For example, complex biogeochemical models include SST when constructing a mathematical framework for studying the ecosystem of the region (e.g., Oguz et al. 2002). In addition, given that SST is an active participant in thermodynamic exchanges from ocean to atmosphere, obtaining accurate SSTs from an OGCM becomes an important issue in the Black Sea, a region with many competing processes that are not accurately known, including air–sea exchange, oceanic transport, and vertical mixing.

In general, an OGCM needs to use the best available turbidity fields to predict upper ocean quantities including the SST (e.g., Murtugudde et al. 2002; Kara et al. 2004). The reason is that the optical properties of the upper ocean can markedly change the dynamical response of the mixed layer to atmospheric forcing, such as wind stress and heat fluxes (Kara et al. 2005a, hereinafter KWH). Not surprisingly, previous modeling studies showed that SST is sensitive to the vertical distribution of the absorbed solar flux (e.g., Schneider and Zhu 1998; Rochford et al. 2001) due to the fact that the upper ocean is relatively transparent to solar radiation. In particular, ~50% of the insolation penetrating the sea surface is composed of wavelengths longer than 780 nm (Morel and Maritorena 2001). The near-infrared radiation is absorbed and converted to heat near the ocean surface. Ultraviolet radiation has a wavelength of <400 nm and forms only a small fraction of the total radiation (Lalli and Parsons 1997). The remaining 50% of the radiation comprises the visible spectrum with wavelengths between 400 and 700 nm that penetrate deeper into the ocean (e.g., Liu et al. 1994). These are approximately the same wavelengths used by plants in photosynthesis, so these wavelengths are commonly referred to as photosynthetically active radiation (PAR).

Given that the attenuation of PAR (k_{PAR}) is very large in the Black Sea all year and the mixed layer depth (MLD) is very shallow, especially in summer (Kara et al. 2005b), an accurate treatment of insolation penetration is needed for Black Sea OGCM studies. This requires the use of spatially and temporally varying turbidity fields. Thus, the Black Sea OGCM studies should use ocean turbidity at high spatial resolution as part of the heat flux forcing. This can be achieved by using remotely sensed attenuation depths in the parameterization of solar subsurface heating. By doing so, the time-varying solar penetration schemes can then treat attenuation as a continuous quantity, which is an improvement over the use of a few discrete attenuation values corresponding to classical Jerlov water types (Jerlov 1976). In fact, KWH also concluded that a single Jerlov water type could not be used for predicting stratification and surface currents in the Black Sea by demonstrating the impact of using a remotely sensed attenuation depth climatology that is applicable to any OGCM that has fine vertical resolution near the surface.

Predicting variations in SST associated with eddies requires eddy-resolving OGCMs. However, there are only a limited number of numerical ocean modeling studies for the Black Sea (Table 1). The OGCMs most commonly used in the Black Sea have been earlier versions of the Princeton Ocean Model (POM) and the Modular Ocean Model (MOM). The POM is a free-

surface primitive equation ocean model for an incompressible, Boussinessq, and hydrostatic fluid (e.g., Blumberg and Mellor 1987). It employs bottom-following σ coordinate and coast-following orthogonal curvilinear coordinate systems and includes the level-2.5 turbulence closure scheme of Mellor and Yamada (1982). The very early version of the *z*-coordinate MOM used in Black Sea model studies (e.g., Stanev et al. 1995; Stanev and Stenava 2001) is based on Bryan (1969). A few other eddy-resolving OGCMs have also been used in the Black Sea studies. For example, Stanev and Beckers (1999) performed Black Sea simulations with the Geohydrodynamics Environment Research (GHER) model, which is based on the primitive equations (Nihoul et al. 1989; Beckers 1991), following a few fine-resolution (5 km $\times$ 5 km) GHER model studies (Grégoire and Lacroix 2001; Beckers et al. 2002). Staneva et al. (2001) examined sea surface circulation using the Dietrich Center for Air–Sea Technology (DieCAST) model, a primitive equation, *z*-level, hydrostatic, fully conservative, and Boussinessq OGCM (Dietrich 1997).

The main focus of the OGCM studies mentioned above (see also Table 1) was to examine the dynamics of the Black Sea ocean circulation and realism of the simulated circulation features. In particular, upper-ocean circulation including the Rim Current system, interior cells involving various gyres, and eddies was examined. These features are well-known characteristics of the upper-ocean Black Sea circulation (e.g., Sur et al. 1994; Korotaev et al. 2001; Zatsepin et al. 2003). However, none of these OGCM studies directly examined SST predictions in the Black Sea or gave any indication of the effect of water turbidity on the OGCM results, the focus of this paper. For this purpose, we use the Hybrid Coordinate Ocean Model (HYCOM) with ~3.2 km resolution in the horizontal and vertical resolution as fine as 3 m near the sea surface. HYCOM uses the layered continuity equation to make a dynamically smooth transition from isopycnal coordinates in the stratified ocean to a terrain-following coordinate in shallow coastal regions, and to *z*-level coordinates in the mixed layer and/or unstratified seas. Such a hybrid coordinate model approach is optimal for the Black Sea because of the steep continental slope and the wide shelf in some regions. HYCOM is designed to make an accurate transition between deep and shallow water, historically a challenging problem for ocean models.

In this paper, our main purpose is threefold: 1) to demonstrate the capability of HYCOM to predict climatological SST on monthly time scales and discuss the effects of two different atmospheric forcing sets on the model simulations, 2) to examine effects of water turbidity and subsurface solar radiation on the SST simulations using a monthly mean attenuation depth climatology as constructed from a remotely sensed dataset, and 3) to perform extensive model–data comparisons using a set of statistical metrics along with evaluation criteria for SST simulation sensitivity to turbidity and solar attenuation depths effects. Accordingly, this paper is organized in the following manner. Section 2 briefly describes the OGCM (HYCOM) used in this paper along with its application to the Black Sea. Section 3 presents the model simulations and discusses the differences between net heat flux at the sea surface and the penetrating heat flux amount based on various water turbidity levels. Section 4 presents SST model–data comparisons. Section 5 investigates a possible linear relationship between sub-mixed-layer heat flux changes and SST changes in the model, and hence the potential impact of sub-mixed-layer heat flux on simulated SST accuracy. Conclusions are given in section 6.

2. Ocean model description

HYCOM has a generalized vertical coordinate as described in Bleck (2002). It behaves like a conventional σ (terrain following) model in very shallow oceanic regions, like a *z*-level coordinate model in the mixed layer or other unstratified regions, and like an isopycnic-coordinate model in stratified regions. The transition between coordinate types is made dynamically in space and time via the layered continuity equation.

The model contains a total of five prognostic equations: two for the horizontal velocity components, a mass continuity or layer thickness tendency equation, and two conservation equations for a pair of thermodynamic variables, such as salt and temperature or salt and density. KWH added a new sea surface energy balance that accounts for spatial and temporal water turbidity as also summarized in section 2a. Here, we present a new parameterization of longwave flux as a relaxation term (see section 2b). Both of these additions are designed to improve the prediction of upper ocean quantities, especially SST.

HYCOM uses a nonslab *K*-profile parameterization (KPP) mixed layer submodel (Large et al. 1994, 1997). The KPP is a first-order turbulence closure ocean surface boundary layer model that is intermediate in computational complexity between bulk mixed layer models and second-order turbulence closures. It is currently the standard mixed layer submodel for HYCOM because it is relatively insensitive to low vertical resolution, and the hybrid coordinate approach tends to require fewer layers/levels than fixed vertical coordinate approaches. The KPP scheme provides mixing from surface to bottom, matching the large surface boundary layer diffusivity/viscosity profiles to the weak diapycnal diffusivity/viscosity profiles of the interior ocean. There are numerous advantages to this model. In the ocean interior, the contribution of background internal wave breaking, shear instability mixing, and double diffusion (both salt fingering and diffusive instability) are parameterized. In the surface boundary layer, the influences of wind-driven mixing, surface buoyancy fluxes, and convective instability are parameterized. The KPP submodel also parameterizes the influence of nonlocal mix-

ing of temperature and salinity, which permits the development of countergradient fluxes. It is semi-implicit, requiring multiple iterations.

a. Surface energy balance

Prior to executing the KPP algorithm, surface fluxes of thermodynamic variables and momentum are distributed entirely over the uppermost model layer, with the exception of penetrating shortwave radiation. Shortwave radiation can penetrate to deeper layers, with the penetration depth depending on water turbidity. The following contains a comparison of the previous HYCOM subsurface heating approach and the one used in this paper.

Traditionally, the two-component (red and blue light) exponential decay model of Jerlov (1976) was used to calculate penetrating shortwave radiation in HYCOM (Halliwell 2004). The depth of penetration was a function of water turbidity, represented by the Jerlov water type, which was same everywhere in time and space. Given the incoming shortwave radiation flux S_0 at the surface, the flux passing through model interface k, located at pressure p_k, was expressed as follows:

$$S_k = S_0\left[r\exp\left(\frac{-p_{k+1}}{\beta_R}\right) + (1-r)\exp\left(\frac{-p_{k+1}}{\beta_B}\right)\right], \quad (1)$$

where r is the fraction of light that is red, β_R is the penetration depth scale of red light, and β_B is the penetration depth scale of blue light. The r values for the classical Jerlov water types (types I, IA, IB, II, and III) are 0.58%, 0.62%, 0.67%, 0.77%, and 0.78%, respectively. The corresponding β_R values are 0.35, 0.60, 1.00, 1.50, and 1.40 m, and similarly, the β_B values are 23.0, 20.0, 17.0, 14.0, and 7.9 m, respectively. Note β_R values increase with increasing turbidity because the fraction of red light also changes.

In this paper, we use the spatially and temporally varying satellite-based attenuation coefficients ($k_{\rm PAR}$) instead of a constant Jerlov value everywhere (Fig. 1). With the new subsurface heating scheme introduced in Kara et al. (2005a), in detail, the net heat flux absorbed from the sea surface down to depth z[$Q(z)$] is parameterized as follows:

$$Q(z) = Q(0) + [Q_{\rm sol}(0) - Q_{\rm sol}(z)], \quad (2)$$

$$Q(0) = Q_{\rm LW} + Q_L + Q_S, \quad (3)$$

$$Q_{\rm sol}(z)/Q_{\rm sol}(0) = (1-\gamma)\exp(-z/0.5) + \gamma\exp(-zk_{\rm PAR}), \quad \text{and} \quad (4)$$

$$\gamma = \max(0.27,\ 0.695 - 5.7k_{\rm PAR}), \quad (5)$$

where $Q(0)$ is net heat flux absorbed at the sea surface, $Q_{\rm sol}(0)$ is total shortwave radiation at the sea surface, $Q_{\rm sol}(z)$ is remaining (unabsorbed) shortwave radiation at depth z, $Q_{\rm LW}$ is the downward net longwave radiation,

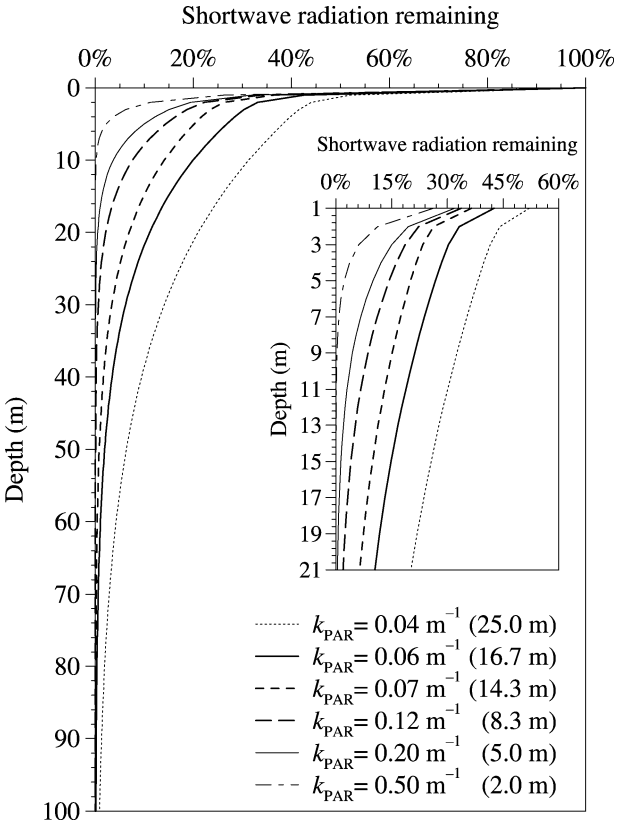

FIG. 1. Percentage of penetrating shortwave radiation remaining below the sea surface vs depth. A few example profiles are shown for a few selected $k_{\rm PAR}$ values: 0.04, 0.06, 0.07, 0.12, 0.20, and 0.50 m^{-1}. The corresponding solar attenuation depths ($k_{\rm PAR}^{-1}$) are given in parentheses. The small panel inside the figure is intended to demonstrate shortwave radiation values remaining below the surface from 1 to 21 m. The HYCOM $k_{\rm PAR}$ values of 0.04345, 0.0500, 0.0588, 0.0714, 0.1266, and 2.00 m^{-1} correspond to Jerlov I, IA, IB, II, III, and mud cases, respectively. It must be emphasized that HYCOM subsurface heating parameterization includes spatially and temporally varying $k_{\rm PAR}$ values rather than the discrete Jerlov water types. The model uses a 0.5-m e-folding depth for the red spectrum. For large $k_{\rm PAR}$ values (e.g., $k_{\rm PAR} > 0.50$ m^{-1}) it matters little what fraction is in the each band because both bands have small e-folding depths of 0.5 m.

Q_L is the downward latent heat flux and Q_S is the sensible heat flux. The HYCOM's ''surface'' heat flux is not $Q(0)$, but rather the near-surface flux absorbed in layer 1 [e.g., Q(3 m) when the top model layer is 3 m thick]. Thus, $Q(0)$ does not include $Q_{\rm sol}(0)$. None of $Q_{\rm sol}(0)$ is absorbed at the surface although $(1-\gamma)$% is absorbed very near the surface. In Eq. (4), the red penetration scale is 2 m, and the blue penetration scale is $1/k_{\rm PAR}$. In summary, the optical-depth-dependent attenuation of subsurface heating in HYCOM involves $k_{\rm PAR}$. Spatial and temporal variability of monthly mean $k_{\rm PAR}$ used in model simulations is further discussed in section 4b.

In Eq. (3), Q_L and Q_S are calculated using model SST and the bulk formulas of Kara et al. (2002) at each model time step. Net solar radiation (net shortwave radiation

plus net longwave radiation) is so dependent on cloudiness that this is taken directly from the European Centre for Medium-Range Weather Forecasts (ECMWF) [or Navy Operational Global Atmospheric Prediction System (NOGAPS)] for use in the model, except for a modification to longwave radiation based on the model SST as discussed in section 2b. Basing fluxes on the model SST automatically provides a physically realistic tendency toward the correct SST. If the model SST is too high or low, the flux is reduced or increased relative to that from the correct SST. The trend toward reality is typically sufficient on its own to keep the model SST approximately on track.

b. Longwave radiation effects on SST

Blackbody longwave radiation into the ocean depends only on SST (T_s) as follows:

$$Q_{\rm bb} = -0.98\sigma(T_s + 273.16)^4, \quad (6)$$

where the Stefan–Boltzmann constant (σ) is 5.67×10^{-8}. There is a negative sign because this is heat lost from the ocean.

The net longwave flux is the sum of this upward blackbody term and the downward atmospheric longwave flux. It is dependent on cloudiness, and this is one reason why OGCMs, such as the Naval Research Laboratory Layered Ocean Model (NLOM) with an embedded mixed layer (Wallcraft et al. 2003), take the net longwave flux as an input atmospheric field. However, the blackbody flux is independent of cloudiness, and it is not clear that the downward atmospheric longwave flux is significantly dependent on SST as opposed to the air temperature. Common approximations of the net longwave flux assume that T_s, air temperature, and cloudiness are all related to the atmospheric longwave flux (e.g., Gupta et al. 1992), but the most recent mid- to high-latitude approximation (Josey et al. 2003) suggests that the atmospheric longwave component depends on air temperature and cloudiness alone.

If we assume that $Q_{\rm bb}$ is the only T_s dependent component of $Q_{\rm LW}$ and that it was calculated with a SST of $T_{\rm so}$, potentially different from the model SST of T_s,

$$Q_{\rm LW}(T_s) = Q_{\rm LW}(T_{\rm so}) + Q_{\rm bb}(T_s) - Q_{\rm bb}(T_{\rm so}), \quad (7)$$

$$Q_{\rm LW}(T_s) = Q_{\rm LW}(T_{\rm so}) + Q'_{\rm bb}(T_s)(T_s - T_{\rm so}), \quad \text{and} \quad (8)$$

$$Q'_{\rm bb} = -0.98\sigma 4.0(T_s + 273.16)^3. \quad (9)$$

Here, it is noted that the approximation (8) is obtained by assuming $(T_s - T_{\rm so})$ is small in (7). The cubic equation (9) is in turn very well approximated by a linear fit over the range from -2 to 32 (Fig. 2). This linear fit is given by

$$Q'_{\rm bb} \approx -4.506 - 0.0554T_s. \quad (10)$$

The total range is small (-4.4 to -6.3 W m^{-2} °C^{-1}). Thus, a constant value of -5.3 W m^{-2} °C^{-1} is a fairly good approximation to the blackbody radiation correction. Overall, this is a much smaller effect than that of SST variations on latent and sensible heat fluxes, already allowed for by HYCOM; however, it is in the right direction (e.g., a warm SST anomaly produces cooling longwave anomaly).

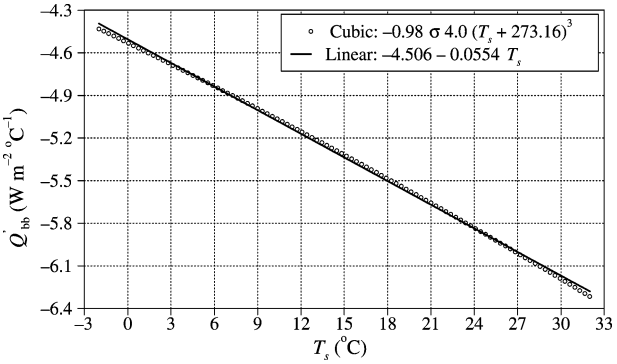

FIG. 2. A linear approximation to the blackbody radiation correction based on the original cubic function. The T_s values shown on the x axis are SSTs from $-2°$ to 32°C, a representative of the global ocean. The Stefan–Boltzmann constant (σ) in the cubic formulation is 5.67×10^{-8}. For simulations using interannual atmospheric forcing, the SST used to derive $Q_{\rm LW}$ is usually available, and it can be read in as an additional "forcing" term. Note that this typically is not an accurate SST on the scales of a high-resolution ocean model. Thus, on the smallest scales this is a genuine and needed longwave correction. For coupled atmosphere–ocean models, the atmospheric model is presumably using the ocean SST and so the correction would be zero if they are both on the same grid. There could still be a longwave correction if the ocean model was on a finer grid than the atmospheric model.

For simulations using climatological atmospheric forcing, it is reasonable to assume that the climatological SST (T_c) was used to generate the longwave flux. The blackbody correction can therefore be approximated as a relaxation term:

$$Q_{\rm LW}(T_s) = Q_{\rm LW}(T_c) - 5.3(T_s - T_c). \quad (11)$$

HYCOM already has such a term, expressed as an equivalent depth (H), for a 30 day e-folding time as follows:

$$Q_{\rm relax} = \frac{(HC_{\rm pw}\rho_0)}{(30 \times 86\,400)}(T_c - T_s), \quad (12)$$

where $C_{\rm pw}$ is specific heat of water (3990 J kg^{-1} K^{-1}) and ρ_0 is the water density (1000 kg m^{-3}). Based on (12), the H must be 3.5 m to get 5.3 W m^{-2} °C^{-1}. Similarly, the H must be 3 m to get 4.6 W m^{-2} °C^{-1}. This relatively small relaxation term is well justified, based on the need for a blackbody correction. All simulations presented in this paper use a H value of 3.5 m.

c. Black Sea model

The Black Sea model has a resolution of $1/25°$ × $1/25°$ cos(lat), (longitude × latitude) (~3.2 km), which is at least a factor of 3 finer grid spacing than most of the earlier OGCM studies shown in Table 1. There are 15 hybrid layers (10 predominantly isopycnal—and

TABLE 2. The six HYCOM simulations performed. The wind and thermal forcing (i.e., air temperature at 10 m, air mixing ratio at 10 m, and shortwave and longwave radiation) are from the 6-hourly ECMWF and FNMOC NOGAPS. There is only weak relaxation to climatological MODAS sea surface salinity in the model simulations. There is no relaxation to an SST climatology and no subsurface relaxation to climatological temperature or salinity. The net freshwater balance (P_{net}) in the model is expressed as $P_{net} = E - P + P_{river} + P_{Bosp.}$, where E is evaporation (due to latent heat flux) calculated at each model time step, P is precipitation due to rain or snow, P_{river} is due to rivers parameterized as precipitation, and $P_{Bosp.}$ is ''negative precipitation'' (i.e., evaporation) due to the transport from the Bosporus Strait. The Bosporus is considered a negative precipitation field to close the evaporation minus precipitation budget in the Black Sea.

Expt	κ_{PAR}	Description of the experiment	Forcing
1	Variable	Spatial and temporal attenuation depths	ECMWF
2	99 m^{-1}	All solar radiation absorbed at the surface	ECMWF
3	0.06 m^{-1}	Clear-water constant attenuation depth of 16.7 m	ECMWF
4	Variable	Spatial and temporal attenuation depths	NOGAPS
5	99 m^{-1}	All solar radiation absorbed at the surface	NOGAPS
6	0.06 m^{-1}	Clear-water constant attenuation depth of 16.7 m	NOGAPS

5 always z—levels) in the model. HYCOM needs fewer vertical coordinate surfaces than, say, a conventional z-level model because isopycnals are more efficient in representing the stratified ocean (see KWH for details). The density values for the isopycnals and the decreasing change in density between isopycnal coordinate surfaces are based on the density climatology from Modular Ocean Data Assimilation System (MODAS) (Fox et al. 2002) as explained in KWH, in detail. The model is also initialized using the temperature and salinity profiles from the MODAS climatology. The bottom topography in the Black Sea model was constructed using various sources, including the 1-min subregion of NAVOCEANO's DBDB-V that covers the Mediterranean Sea, including the Aegean Sea and Black Sea. It was first interpolated to the model grid; then, smoothed twice with a nine-point real smoother to reduce topographic energy generation at scales poorly resolved by the model.

The climatological atmospheric forcing fields read into the model are wind stress and thermal forcing (air temperature and air mixing ratio at 10 m above the sea surface, net shortwave radiation at the sea surface, and net solar radiation, which is the sum of net shortwave radiation and net longwave radiation at the sea surface). The model simulations presented in this paper use wind/thermal forcing from two different archived weather center products: 1) the 1.125° × 1.125° ECMWF reanalysis (ERA; Gibson et al. 1997), which spans 1979–93, and 2) the 1.0° × 1.0° Fleet Numerical Meteorology and Oceanography Center (FNMOC) NOGAPS from 1998 to 2002 (Rosmond et al. 2002). All model simulations were performed using climatological monthly mean forcing fields. However, a high-frequency wind stress component was added to the climatological wind forcing because monthly winds do not produce realistic MLDs (Wallcraft et al. 2003). The net heat flux at a given depth in the model includes effects of turbidity through the monthly k_{PAR} fields based on the Sea-Viewing Wide Field-of-View Sensor (SeaWiFS) as shown in section 2a.

The model treats rivers as a runoff addition to the surface precipitation field, which is also used for the evaporation minus precipitation budget. The river flow is first applied to a single ocean grid point and smoothed over surrounding ocean grid points, yielding a contribution to precipitation in meters per second. In the Black Sea model, there are a total of six major rivers (Danube, Dniepr, Rioni, Dniestr, Sakarya, and Kizilirmak) whose monthly mean climatological river discharge values were obtained from the readily available River Discharge (RivDIS) dataset (Vörösmarty et al. 1997).

3. Model simulations and mixed layer flux

All HYCOM simulations (Table 2) presented in this paper are performed with no assimilation of any ocean data except initialization to climatology. There is only weak relaxation to sea surface salinity. There is no relaxation to a SST climatology and no subsurface relaxation to climatological temperature or salinity. The model is run until it reaches statistical equilibrium using climatological monthly mean thermal atmospheric forcing, but the wind forcing includes 6-hourly variability. It takes about 5–8 model years for a simulation to reach the statistical equilibrium for all parameters.

Climatologically forced model simulations that use three different k_{PAR} values were performed to investigate the effects of ocean turbidity on SST (Table 2). For experiment (expt) 1 (the standard simulation), spatially and monthly varying k_{PAR} values interpolated to the HYCOM grid are used. For experiment 2, all of the solar radiation is absorbed in the mixed layer by using a very large k_{PAR} value of 99.9 m^{-1}. For experiment 3, the water turbidity over the Black Sea is set to a constant, $k_{PAR} = 0.06\ m^{-1}$, which is a representative value for clear water over the global ocean (e.g., Kara et al. 2004). Experiments 1, 2, and 3 use wind/thermal forcing from the ECMWF, while 4, 5, and 6 are essentially twins of 1, 2, and 3 but using wind/thermal forcing from the NOGAPS. In experiments 3 and 6 the e-folding penetration depth of k_{PAR}^{-1} is 16.7 m. This is close to values used in recent OGCM studies: 17 m (Murtugudde et al. 2002) and 23 m (Nakamoto et al. 2001). Experiments 2 and 5, which assume all radiation absorbed at the sea surface, represent a traditional OGCM approach (e.g., Yuen

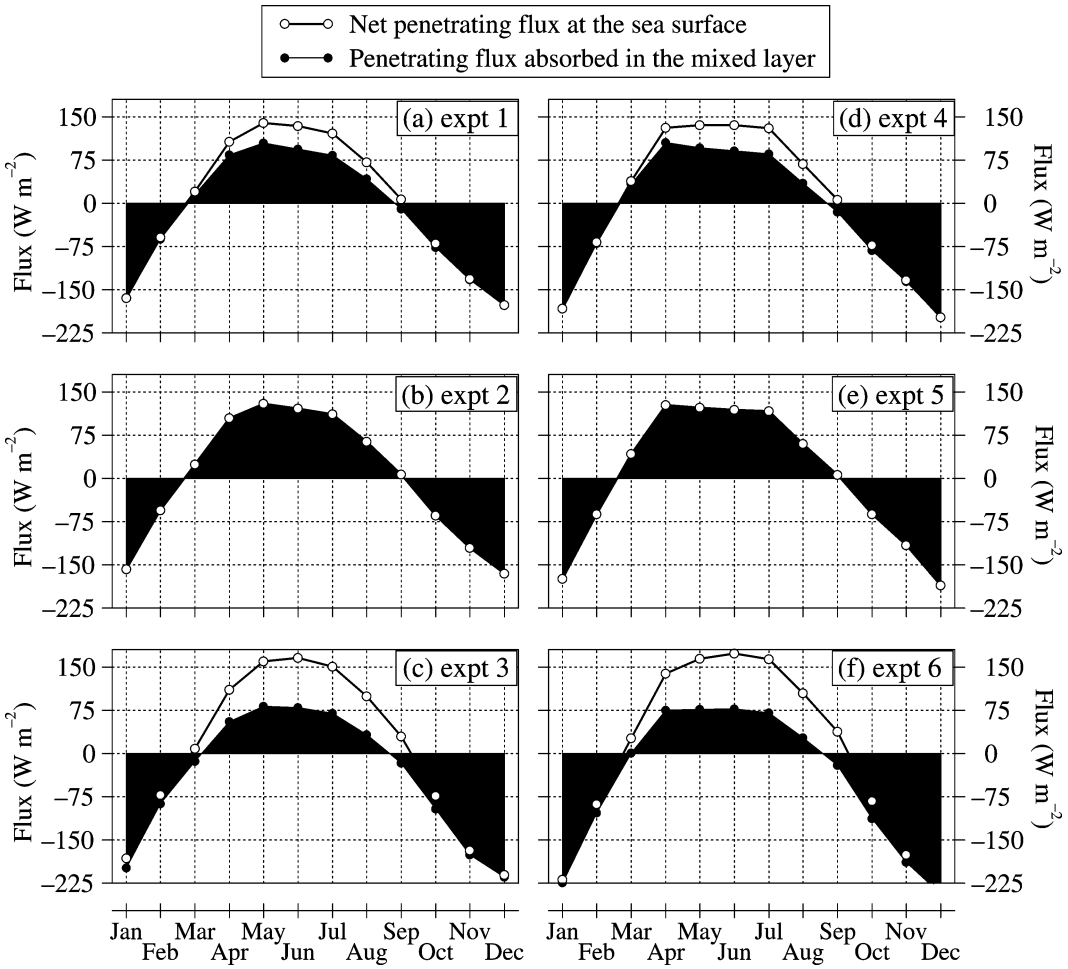

FIG. 3. The basinwide monthly mean net penetrating heat flux at the sea surface and the penetrating heat flux absorbed in the mixed layer for HYCOM simulations forced with the climatological ECMWF wind/thermal fluxes (expts 1, 2, and 3) and NOGAPS wind/thermal fluxes (expts 4, 5, and 6). The difference between these two curves is the shortwave radiation absorbed below the mixed layer. See Table 2 for a description of each simulation. The monthly means were formed from the last 4 years of the simulations during model years 5–8. Note that monthly mean flux values were formed using daily model fluxes. The negative sign represents heat loss from the ocean. The largest difference between the net penetrating heat flux at the sea surface and the heat flux in the mixed layer occurs in Jun when the shortwave radiation below the mixed layer is 40, 86, 44, and 97 W m^{-2} for expts 1, 3, 4, and 6, respectively.

et al. 1992). By using a k_{PAR} value of 0.06 m^{-1}, the major purpose is to demonstrate how SST would be affected if the Black Sea were included as part of a global ocean model (or Atlantic model) using the clear water constant attenuation depth assumption.

Before investigating the possible effects of water turbidity on the SST, we first calculate basinwide mean heat fluxes in the Black Sea (Fig. 3). The mixed layer flux is the heat flux applied to the mixed layer in the model simulations. The difference between the basinwide mean heat flux at the sea surface and mixed layer flux is the shortwave radiation absorbed below the mixed layer. Experiments 2 and 5 assume all radiation at the sea surface so the basinwide mean heat flux is equal to the mixed layer flux in these simulations. The basinwide annual-mean net heat flux at the sea surface is zero for all experiments because the Black Sea has closed boundaries. Essentially, a model at equilibrium must have zero net surface flux, and in HYCOM this is maintained using the bulk parameterizations (see section 2a). The bulk heat flux parameterization provides a physically realistic feedback between SST and net fluxes. Any climatologically (i.e., repeated year) forced case will have zero annual net heat flux, with the annual mean SST automatically adjusting to make this happen. Therefore, any annual mean error will be in SST, rather than in the heat flux balance.

The basinwide annual-mean heat fluxes below the mixed layer are 17 and 40 W m^{-2} for experiments 1 and 3, respectively. Similarly, they are 20 and 47 W m^{-2} for experiments 4 and 6. Overall, the clear-water constant attenuation-depth assumption (i.e., expts 3 and

6) results in a larger net flux below the mixed layer over the Black Sea. Large shortwave radiation absorbed below the mixed layer is only seen in spring and summer (Fig. 3).

4. HYCOM–data comparisons

In this section, several statistical metrics are used to intercompare monthly mean SSTs obtained from the climatologically forced HYCOM simulations (expts 1–6) and to compare them with a satellite-based climatological SST dataset at each model grid point of the Black Sea. These comparisons are designed to examine the sensitivity of model SST to water turbidity. For evaluation of the model results, monthly mean SSTs are formed from daily fields using the last four model years (years 5–8). An example of a daily SST snapshot is shown in Fig. 4a to demonstrate the impact of eddies on SST from the fine-resolution (3.2 km) Black Sea HYCOM. At least a 4-yr model mean was needed because HYCOM with 3.2-km resolution has a strong nondeterministic component due to flow instabilities. These are a major contribution to the simulated Black Sea circulation and SST at this resolution.

Given that all forcing in the HYCOM simulations is climatological, monthly mean HYCOM SSTs can be compared with climatological monthly mean SSTs. The climatological SST used in this paper is the Pathfinder dataset (Casey and Cornillon 1999), which is based directly on satellite data during 1985–97. It has a resolution of 9.28 km (~9 km). The annual-mean Pathfinder SST climatology interpolated to the HYCOM domain is shown in Fig. 4b. The climatology was created by averaging daily fields into monthly means. Both daytime and nighttime daily fields are included in each monthly average. A 7×7 median filter is applied to fill in many of the gaps, and a 7×7 median smoother is used for the entire field to remove small-scale noise. The Pathfinder climatology is preferred for the HYCOM model comparisons for two main reasons: 1) As explained in Casey and Cornillon (1999), the Pathfinder climatology outperforms the commonly used climatologies, such as the $1^\circ \times 1^\circ$ Met Office Global Ice and Sea Surface Temperature (GISST) climatology (Rayner et al. 1996); the $1^\circ \times 1^\circ$ *World Ocean Atlas 1994* (WOA94) climatology (Levitus and Boyer 1994), which does not include the Black Sea at all; and the $1^\circ \times 1^\circ$ National Oceanic and Atmospheric Administration (NOAA) optimal interpolation (OI) SST climatology (Smith and Reynolds 1998), shown in Fig. 4b, and 2) it has much finer resolution than the others, which is appropriate for the fine-resolution Black Sea model used in this paper.

Other observed climatological data sources are available to validate HYCOM SST, such as the later version of the NOAA optimal interpolation SST climatology (Reynolds et al. 2002) and the Comprehensive Ocean–Atmosphere Data Set (COADS) SST climatology (da Silva et al. 1994). However, they are still on the $1^\circ \times 1^\circ$ grid. Even though the MODAS climatology described in section 2c has sufficiently fine resolution to validate HYCOM SST results, it is a bimonthly dataset and was already used in the model initilization. Thus, it is not used for the model–data comparisons.

Here it is noted that annual-mean SST biases between the Pathfinder climatology and NOAA OI climatology are not larger than 0.5°C in most of the region except over the northwestern shelf where there is an annual mean bias up to 2°C (Fig. 4b). However, there is a basin-averaged ECMWF–NOGAPS bias (rms difference) of 0.74°C (1.45°C) between monthly mean air temperatures at 10 m above the sea surface from ECMWF and NOGAPS over the annual cycle (see section 4a for definitions of bias and rms difference). This is significant because 10-m air temperatures are used in the model simulations as part of the thermal forcing.

a. Statistical metrics

Different statistical measures are considered together to measure the strength of the relationship between SST values predicted by the model (HYCOM SST) and those from the climatology (Pathfinder SST). The latter is interpolated to the model grid for model–data comparisons. We evaluate time series of monthly mean SST at each model grid point over the Black Sea. Following Murphy (1988), the statistical relationship used in comparisons between the 12 monthly mean Pathfinder SST (X) and HYCOM SST (Y) can be expressed as follows:

$$\mathrm{ME} = \overline{Y} - \overline{X}, \tag{13}$$

$$\mathrm{rms} = \left[\frac{1}{n}\sum_{i=1}^{n}(Y_i - X_i)^2\right]^{1/2}, \tag{14}$$

$$R = \frac{1}{n}\sum_{i=1}^{n}(X_i - \overline{X})\frac{(Y_i - \overline{Y})}{(\sigma_X\sigma_Y)}, \quad \text{and} \tag{15}$$

$$\mathrm{SS} = R^2 - \underbrace{\left[R - \left(\frac{\sigma_Y}{\sigma_X}\right)\right]^2}_{B_{\mathrm{cond}}} - \underbrace{\left[\frac{(\overline{Y} - \overline{X})}{\sigma_X}\right]^2}_{B_{\mathrm{uncond}}}, \tag{16}$$

where $n = 12$, ME is the mean error, rms is the root-mean-square difference, R is the correlation coefficient, SS is the skill score, and $\overline{X}(\overline{Y})$ and $\sigma_X(\sigma_Y)$ are the mean and standard deviations of the Pathfinder (HYCOM) SST values, respectively. For the 12 monthly SST fields at each grid point over the Black Sea, the R value between HYCOM and Pathfinder SST must be at least ± 0.53 for it to be statistically different from a R value of zero based on the Student's t test at the 95% confidence interval (Neter et al. 1988).

The nondimensional SS, given in (16), measures accuracy by including conditional and unconditional biases (Murphy 1992). It is used for the model–data comparisons because one needs to examine more than the shape of the seasonal cycle, measured using R (and SS).

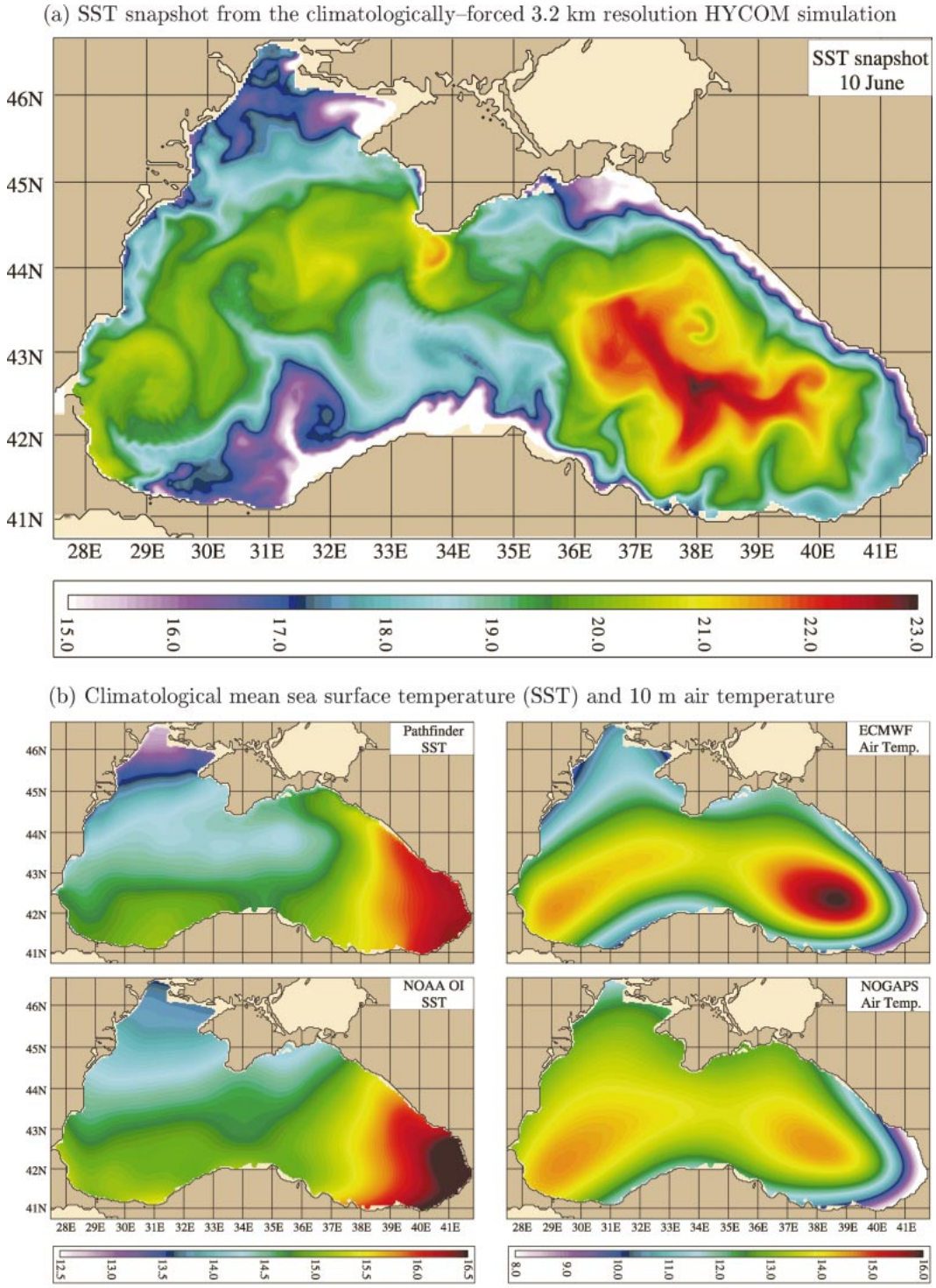

FIG. 4. (a) Snapshot of climatologically forced SST on 10 Jun, which was obtained from the HYCOM simulation forced with ECMWF wind/thermal fluxes. (b) Climatological mean SST and air temperature at 10 m above the sea surface (T_a) from various products: 9-km Pathfinder SST climatology, which can be accessed through the Earth Observing System Data and Information System (EOSDIS) Physical Oceanography Distributed Active Archive Center (PO.DAAC) at the Jet Propulsion Laboratory (JPL), $1° \times 1°$ NOAA SST climatology, which was developed at the Climate Prediction Center, T_a from $1.125° \times 1.125°$ ERA, and T_a from $1° \times 1°$ FNMOC NOGAPS. Annual mean T_a values are over 1979–93 for ECMWF and 1998–2002 for NOGAPS. All fields shown are interpolated to the Black Sea HYCOM domain.

The conditional bias (B_{cond}) is the bias in standard deviation of the HYCOM SST, while the unconditional bias (B_{uncond}) is the mismatch between the mean HYCOM and Pathfinder SST. A simple definition for SS, based on rms difference, is $\text{SS} = 1 - (\text{rms})^2/\sigma_X^2$ as given in Murphy and Daan (1985). The value of R^2 can be considered a measure of ''potential'' skill, that is, the skill that one can obtain by eliminating bias from the HYCOM SST. To have skill the model must have $\text{SS} > 0$, and $\text{SS} = 1$ is perfect skill. Part of the reduction in SS values in comparison to R stems from the squaring of correlation in the SS calculation. Biases are taken into account in the rms differences, but the latter can be small where SS and R are poor because the amplitude of seasonal cycle may be small at some locations.

b. SST predictions from HYCOM

The sensitivity of HYCOM SST to water turbidity is first examined using annual bias (i.e., ME) maps between the HYCOM simulations. Climatological annual mean SST from each experiment is formed (Fig. 5a), and the departure of HYCOM SST from the 9-km Pathfinder SST is calculated (Fig. 5b). Overall, the SST errors in the interior are usually smaller than those along continental boundaries, and the ME for the standard simulations (expts 1 and 4) that use SeaWiFS-based spatially and temporally varying attenuation depths is usually less than ± 0.5°C in the interior of the Black Sea. In fact, the basin-averaged annual ME values are -0.54°, -0.49°, and -0.85°C for experiments 1, 2, and 3, respectively. Similarly, they are 0.19°, 0.25°, and -0.07°C for 4, 5, and 6.

While the ME is small in experiment 6, which assumes the clear-water constant attenuation depth, rms difference and (1 − SS) values are relatively large based on the basin-averaged SST error statistics (Table 3), clearly indicating the importance of using various statistical metrics in deciding which experiment performed best. When using monthly varying attenuation depth rather than a clear-water constant attenuation depth of 16.7 m, HYCOM performance in predicting SST increases significantly. In the case of ECMWF wind/thermal forcing, the basin-averaged rms difference increases ~46%, from 1.41°C (expt 1) to 2.06°C (expt 3). Similarly, in the case of NOGAPS wind/thermal forcing, the basin-averaged rms difference increases ~36%, from 1.39°C (expt 4) to 1.89°C (expt 6), much larger than the annual mean biases. Although the difference in the basin-averaged annual mean SST bias is small between two simulations using the same atmospheric forcing product (e.g., expt 1 vs expt 3 and expt 4 vs expt 6), there are large biases up to 3°C in some individual months. In winter, the mean errors (i.e., expt 3 − expt 1 and expt 6 − expt 4) are usually positive (warmer winter SST when Black Sea turbidity is neglected), while the mean difference is usually negative in summer. Thus, the clear-water assumption gives fairly small annual mean error, with a winter warm bias and the summer cool bias tending to cancel each other out. This lower amplitude in the SST seasonal cycle is reflected in a relatively large conditional bias with respect to the monthly mean Pathfinder SST climatology (Table 3).

Before examining individual monthly mean SST results from various simulations, we first show basin-averaged monthly mean k_{PAR} values (Fig. 6) as processed from the daily averaged k_{490} dataset from SeaWiFS over the Black Sea during 1997–2001. The basin-averaged k_{PAR} ranges from 0.14 m^{-1} in July to 0.26 m^{-1} in December, demonstrating substantial seasonal turbidity variability in the Black Sea. The reader is referred to Kara et al. (2005b) for a detailed examination of spatial and temporal k_{PAR} variability over the Black Sea. The climatological mean of k_{PAR} fields in February and June have a similar pattern and amplitude (Fig. 7a) with basin-averaged values of 0.18 and 0.16 m^{-1}. In general, the smallest k_{PAR} values are usually seen in the easternmost part, with typical attenuation depth (k_{PAR}^{-1}) values ranging from 5 to 10 m. Earlier Black Sea studies (Grégoire et al. 1998; Oguz et al. 2001) reported a light absorption coefficient of ~0.08 m^{-1}. However, our results based on the SeaWiFS clearly demonstrate that absorption coefficients of 0.08 m^{-1} are usually representative of water around the Turkish coast, well below the basin-averaged annual mean k_{PAR} value of 0.19 m^{-1}. Not surprisingly, observational studies are based on limited measurements taken by cruises in the Black Sea, so they do not represent the spatial and temporal variability well.

Given that the amount of solar radiation below the mixed layer in summer is quite large based on the specification of water turbidity as discussed previously (see Fig. 3), one would expect larger SST differences between the experiments in June than in February. This is evident from the HYCOM simulations (Figs. 7b,c). In comparison with standard simulations (expts 1 and 4), absorbing all radiation at the sea surface (expts 2 and 5) results in a negligible cold bias for both atmospheric forcing product in February. During this month the basin-averaged SSTs from experiments 2 and 5 are 0.2° colder than those from experiments 1 and 4 (Table 4). On the other hand, the clear-water assumption (expts 3 and 6) yields SSTs that are ~0.7°C warmer than those from the standard simulations in February. The warm SSTs are because of relatively deep model MLDs (not shown), and thus the relatively low amplitude of the SST seasonal cycle as discussed earlier.

When HYCOM SST from the standard simulation is compared with the ~9-km-resolution Pathfinder SST climatology, the model usually gives a warm bias. The HYCOM SST prediction in the northwestern shelf shows significant differences in accuracy depending on the atmospheric forcing product. While there is almost no bias (or a slightly warm bias) in the NOGAPS wind/thermal forcing case, a relatively large cold SST bias

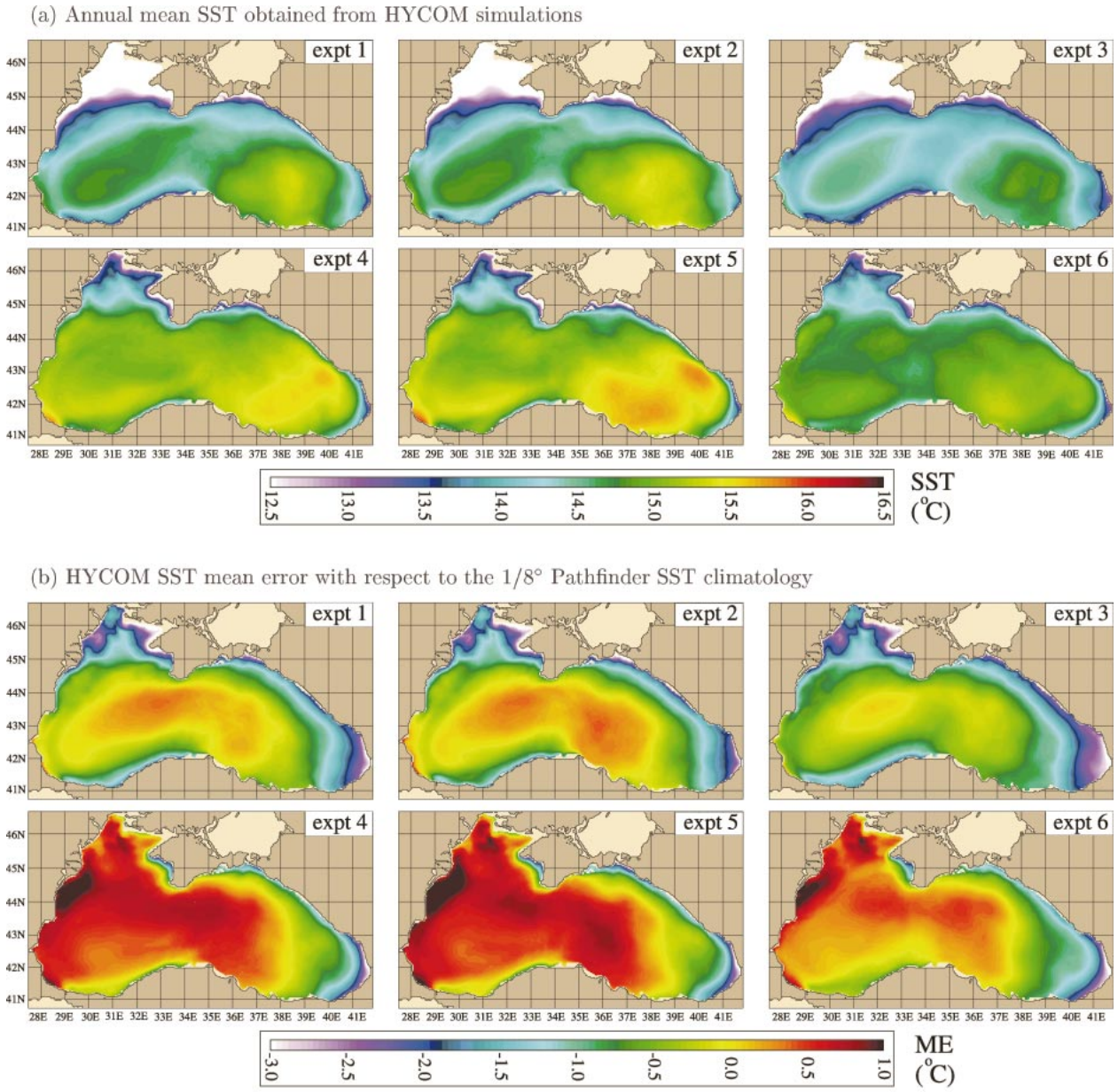

FIG. 5. Model SST comparisons: (a) Annual mean HYCOM SST, and (b) annual mean bias (i.e., ME) with respect to the satellite-based Pathfinder SST climatology, which has a resolution of ~9 km. Expts 1 and 4 represent the standard simulations that use spatially and temporally varying attenuation of PAR (k_{PAR}). Note that expts 1, 2, and 3 are forced with ECMWF wind/thermal fluxes, and expts 4, 5, and 6 are forced with NOGAPS wind/thermal fluxes. All model simulations are performed with no assimilation of or relaxation to SST or any other ocean data.

is evident in the ECMWF wind/thermal forcing case, indicating an effect of the atmospheric forcing product on the model simulations. The big difference in SST is generally attributed to the difference in solar radiation between the two products and to the different land–sea masks used in the products (see section 4c). As evident from spatial plots of shortwave radiation (KWH), the annual mean difference between ECMWF and NOGAPS can be as large as 70 W m^{-2} in the northwestern shelf.

The effects of water turbidity on the SST predictions from HYCOM are largest in June (up to 3°C), and the differences between the experiments change sign from February (Fig. 7c). The assumption of all radiation at the sea surface results in a systematic warm bias over the Black Sea in comparison with the standard experiments, 0.7°C for ECMWF and 0.6°C for NOGAPS forcing. However, there are much larger SST deviations from the standard experiments when using a clear-water constant attenuation depth of 16.7 m in the model sim-

TABLE 3. Basin-averaged SST verification statistics for the six HYCOM simulations performed. In addition to expts 1–6, two additional simulations (one simulation forced with wind/thermal forcing from ECMWF and another simulation forced with wind/thermal forcing from NOGAPS) were performed using a κ_{PAR} value of 0.19 m^{-1}, which represents the SeaWiFS space–time mean for the Black Sea during 1997–2001. The ME, rms, SS, and R values are −0.52°C, 1.67°C, 0.93, and 0.99 for the ECMWF-forced simulation, and 0.15°C, 1.52°C, 0.93, and 0.99 for the NOGAPS-forced simulation, respectively. The reader is referred to section 4a for a detailed description of the statistical measures. Statistics are calculated using monthly mean values. All R values are greater than 0.97 and statistically significant in comparison with a 0.7 correlation value at a 95% confidence interval. Note that a correlation coefficient of 0.98 is not statistically different from a correlation coefficient of 0.99. It is also seen that the basin-averaged annual mean SST bias with respect to the Pathfinder SST climatology is very small, indicating that any initial heat flux bias was also small in the HYCOM simulations.

Expt	ME (°C)	Rms (°C)	B_{cond}	B_{uncond}	SS	R
1	−0.54	1.41	0.017	0.020	0.95	0.99
2	−0.49	1.41	0.010	0.018	0.95	0.99
3	−0.85	2.06	0.068	0.028	0.89	0.99
4	0.19	1.39	0.019	0.011	0.95	0.99
5	0.25	1.45	0.010	0.011	0.95	0.98
6	−0.07	1.89	0.071	0.010	0.91	0.99

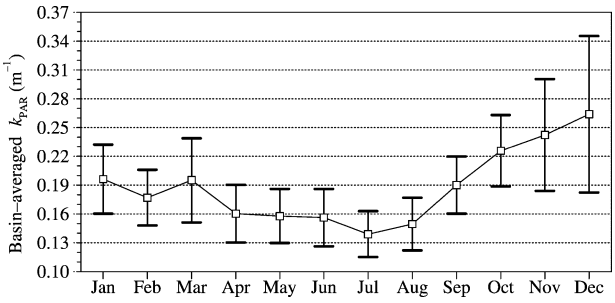

FIG. 6. Basin-averaged monthly mean k_{PAR} (m^{-1}) values along with ± standard deviations in the Black Sea. Monthly mean was formed using daily k_{PAR} values as obtained from SeaWiFS data over 1 Oct 1997–31 Dec 2001. The corresponding monthly mean attenuation depth (i.e., k_{PAR}^{-1}) values are 5.1, 5.7, 5.1, 6.2, 6.3, 6.4, 7.2, 6.7, 5.2, 4.4, 4.1, and 3.8 m from Jan through Dec. The climatological annual mean k_{PAR} value is 0.19 m^{-1} over the annual cycle, which corresponds to an attenuation depth of 5.3 m in the Black Sea.

ulations (expts 3 and 6), cold biases of −2.1°C (−1.7°C) using ECMWF (NOGAPS) forcing (Table 4). Obviously, the very shallow summer MLD is the main reason for seeing these large SST differences. For example, basin-averaged MLD values in February are 43 and 46 m for experiments 3 and 6, respectively, while basin-averaged mean MLD values in June are only 4.1 and 4.6 m. The latter values are more than 4 times shallower than the clear-water constant attenuation depth of ~16.7 m used in experiments 3 and 6. Based on the optimal MLD definition of Kara et al. (2000), the Black Sea has MLDs as shallow as 3 m in summer (e.g., Kara et al. 2005b), and this is much shallower than in most other regions of the global ocean (Kara et al. 2003).

HYCOM skill in reproducing the climatological SST is now evaluated in terms of rms SST difference and SS, statistics described in section 4a. The results in Fig. 8a demonstrate that experiments 1 and 2 give relatively small rms SST differences. They are also small in comparison to the standard deviation of the Pathfinder SST (6.4°C) over the annual cycle. This is especially evident in the interior of the Black Sea. Large rms differences exist in experiment 3, which uses a clear-water constant attenuation depth assumption. In this case, rms differences >3°C are noted along continental boundaries in the eastern part of the Black Sea.

HYCOM SST errors in the easternmost part of the Black Sea are usually attributed to the atmospheric forcing. For example, Schrum et al. (2001) confirmed that the ECMWF output agrees with local datasets in the Black Sea very well. However, one of their major results is that air temperature at 10 m above the sea surface from ECMWF is too low in the easternmost part of the Black Sea. Not surprisingly, this is reflected in the ECMWF-forced experiments, with corresponding large and cold HYCOM SST biases (Fig. 5b). Given that air temperatures from ECMWF and NOGAPS are almost identical in the easternmost part (see Fig. 4b), HYCOM simulation experiments 4, 5, and 6 using atmospheric forcing from FNMOC wind/thermal fluxes yield rms SST difference values similar to ECMWF-forced experiments 1, 2, and 3. This indicates that the NOGAPS product has a similar air temperature bias in the easternmost Black Sea. As will be explained in section 4c, such coastal region errors in the atmospheric forcing are largely due to the land/sea mask used in the ECMWF and NOGAPS products themselves.

When using the NOGAPS wind/thermal forcing (expts 4, 5, and 6), rms SST differences are similar to those using the ECMWF wind/thermal forcing. The rms differences when using the monthly varying attenuation depths are nearly the same as the simulations that assume all radiation absorbed at the sea surface (expts 2 and 5), although these simulations can have SST differences of 1° or 2°C in summer either with ECMWF (expt 2 − expt 1) or NOGAPS (expt 5 − expt 4) forcing (Fig. 7c). The clear-water constant attenuation depth assumption (expts 3 and 6) consistently results in the largest rms differences with respect to the Pathfinder SST climatology (Table 3). The rms difference values for simulations forced by ECMWF and NOGAPS are similar in most regions, usually with slightly lower values for ECMWF than NOGAPS. However, there is a striking difference over the northwest shelf, a region of relatively good agreement for NOGAPS (rms < 1°C) but poor agreement for ECMWF (rms > 1°C) (see section 4c for further explanation). This difference is so large that, despite lower rms differences over most of the domain with ECMWF forcing, the basin-averaged rms SST difference is almost the same as with NOGAPS forcing (Table 3). In particular, zonally averaged rms SST differences and ME for the NOGAPS-forced sim-

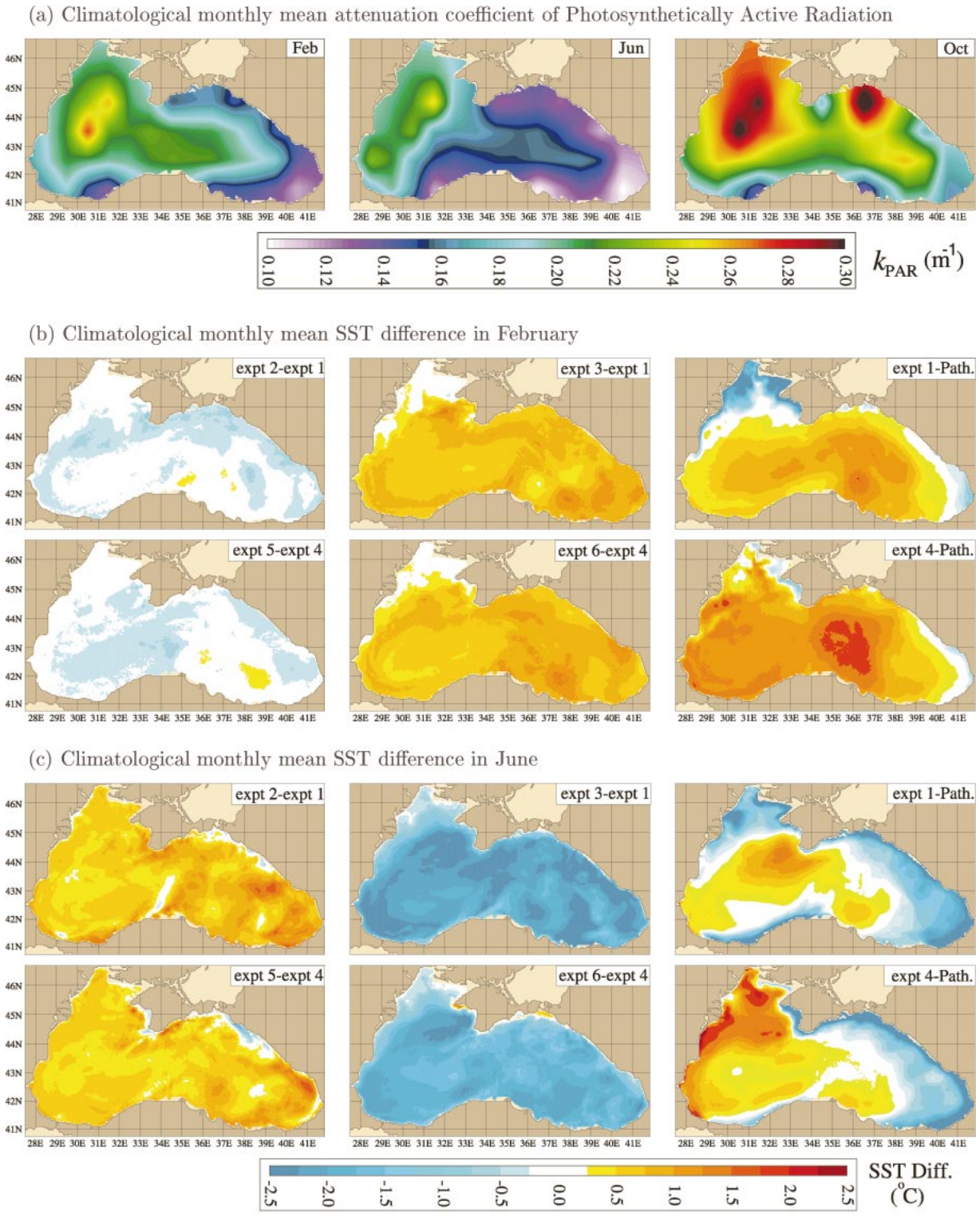

FIG. 7. (a) Spatial variability of climatological monthly mean k_{PAR} over the Black Sea as determined from the SeaWiFS data during 1 Oct 1997–31 Dec 2001. Also shown are monthly mean SST differences between HYCOM simulations along with comparisons with the Pathfinder SST climatology: (b) Feb and (c) Jun. Expts 1 and 4 represent the standard simulations that use spatially and temporally varying attenuation of PAR (k_{PAR}). Note that expts 1, 2, and 3 are forced with ECMWF wind/thermal fluxes, and expts 4, 5, and 6 are forced with NOGAPS wind/thermal fluxes. The observed climatological SST (Path.) is the satellite-based 9-km Pathfinder SST climatology. All model simulations are performed with no assimilation of or relaxation to SST or any other ocean data.

TABLE 4. Basin-averaged monthly mean SST differences between various experiments (see Table 2 for a description of each simulation). Also given are the basin-averaged SST differences between the standard simulations (i.e., expts 1–4) and the 9-km climatological Pathfinder SST (Path.) as described in the text. Coldest and warmest SST differences that are seen over the Black Sea are also given to show how cold/warm these differences can be. In summer, HYCOM SST is very cold in comparison with the Pathfinder SST climatology. This implies that the mixed layer is too deep. Currently, HYCOM has a top layer thickness of 3 m, and using a 1-m top layer in future model simulations would help in reducing these large biases from the model.

SST difference	Jan	Feb	Mar	Apr	May	Jun	Jul	Aug	Sep	Oct	Nov	Dec
						Mean (°C)						
Expt 2–expt 1	−0.2	−0.2	−0.1	0.2	0.6	0.7	0.4	0.3	0.1	−0.1	−0.3	−0.3
Expt 3–expt 1	0.8	0.7	0.5	−0.3	−1.4	−2.1	−1.6	−1.3	−1.0	−0.1	1.0	0.8
Expt 1–Path.	0.5	0.6	0.2	0.3	0.4	−0.4	−1.6	−2.1	−1.8	−1.8	−1.2	0.3
Expt 5–expt 4	−0.2	−0.2	−0.1	0.2	0.5	0.6	0.5	0.3	0.1	−0.2	−0.4	−0.3
Expt 6–expt 4	0.8	0.7	0.6	−0.4	−1.3	−1.7	−1.4	−1.3	−1.2	0.2	1.1	0.9
Expt 4–Path.	1.0	1.2	0.9	1.8	1.6	0.1	−0.7	−1.4	−1.1	−1.3	−0.6	0.8
						Minimum (°C)						
Expt 2–expt 1	−0.8	−1.2	−1.4	−0.5	−0.6	−0.8	−2.4	−2.1	−1.0	−1.0	−1.1	−0.9
Expt 3–expt 1	−0.3	−0.3	−0.4	−0.8	−2.3	−2.9	−2.7	−2.9	−2.1	−1.8	−0.1	−0.1
Expt 1–Path.	−1.5	−1.0	−1.6	−1.9	−1.6	−1.8	−2.6	−2.4	−1.9	−1.5	−1.3	−0.8
Expt 5–expt 4	−0.9	−0.7	−0.5	−0.5	−1.2	−2.6	−1.8	−2.5	−0.9	−1.0	−1.3	−0.9
Expt 6–expt 4	−0.1	−0.2	−0.3	−1.0	−2.2	−3.0	−2.6	−2.6	−2.0	−0.8	0.1	−0.1
Expt 4–Path.	−1.2	−1.2	−1.1	−0.5	−1.1	−2.9	−2.3	−2.5	−1.7	−1.9	−1.7	−1.6
						Maximum (°C)						
Expt 2–expt 1	0.6	0.4	0.5	0.9	1.5	1.7	1.4	1.7	1.1	0.8	0.4	0.3
Expt 3–expt 1	1.3	1.4	1.1	0.7	0.3	0.3	0.9	1.7	1.6	2.3	1.7	1.4
Expt 1–Path.	1.9	1.8	1.3	1.6	2.3	2.3	1.4	−0.1	−0.2	0.7	1.4	2.1
Expt 5-expt 4	0.5	0.4	0.3	0.9	1.3	1.8	1.9	1.4	0.8	0.3	0.4	0.4
Expt 6–expt 4	1.5	1.4	0.9	0.5	0.7	2.3	2.9	1.8	1.3	1.5	2.1	1.7
Expt 4–Path.	2.1	2.0	1.9	3.0	3.2	3.2	1.4	0.6	1.7	2.2	1.9	2.7

ulations are much smaller than those for the ECMWF-forced simulations north of 45°N (Fig. 9).

HYCOM success in predicting SST is especially evident from the SS maps that show values close to 1 in the standard simulations (expts 1 and 4) over most of the Black Sea (Fig. 8b). Although HYCOM simulates the SST seasonal cycle quite well, the SST warms and cools too fast, introducing a phase error (Table 4). The assumption of all radiation absorbed at the surface (expts 2 and 5) as opposed to the standard cases using variable attenuations depths does not significantly affect the SS. In contrast, SS values obtained from the simulations that use the clear-water constant attenuation depths (expts 3 and 6) are relatively low. Similar to the rms difference map (Fig. 8a), the most obvious feature of the SS maps is that the water turbidity does not have any significant effect over the northwestern shelf. The main reason for not seeing any turbidity effects is that the MLD from all simulations is essentially same in all months. The MLD is also deep enough that it nearly encompasses the entire water column over the shelf region during winter (not shown). During summer the heating below the mixed layer is less affected by the turbidity because the depth of solar penetration is more limited by the depth of the shelf rather than turbidity. Consistent with the rms difference, the NOGAPS wind/thermal forcing gives the highest model SS for SST in the northwestern shelf (Fig. 9). In fact, the highest SS values in experiment 4 (see Fig. 8b) are seen on the northwestern shelf north of ≈45°N, while the lowest SS values in experiment 1 are evident at this region. Note that SS is never negative in any of the experiments, and the lowest SS value (0.48) is seen in experiment 3. Any positive SS value is considered as representative of a successful prediction.

Finally, two additional model simulations were performed using the same two atmospheric forcing sets and a constant k_{PAR} value of 0.19 m^{-1}, the climatological annual space–time mean for the Black Sea from SeaWiFS data (Fig. 6). These yield slightly degraded results in comparison to the standard simulations (expts 1 and 4). For example, the basin-averaged rms SST differences with respect to the Pathfinder climatology are 1.67°C (1.52°C) with ECMWF (NOGAPS) wind/thermal fluxes, 18% (11%) larger than values of 1.41°C (1.39°C) obtained from experiment 1 (expt 4), which uses spatially and temporally varying satellite-based solar attenuation coefficients from SeaWiFS.

It must be emphasized that based on results from NLOM with an embedded mixed layer (Kara et al. 2004), it was found that the standard spatially and temporally varying k_{PAR} simulation was closer to the clear-water constant attenuation depth case ($k_{\mathrm{PAR}} = 0.06\ \mathrm{m}^{-1}$) because the global ocean is not very turbid on average and because globally NLOM's mixed layer was relatively deep (including a 10-m minimum). However, in some regions global NLOM results were accurate with all the radiation absorbed in the mixed layer. In the Black Sea, the standard experiments that use space/time variation in attenuation depths (expts 1 and 4) are much

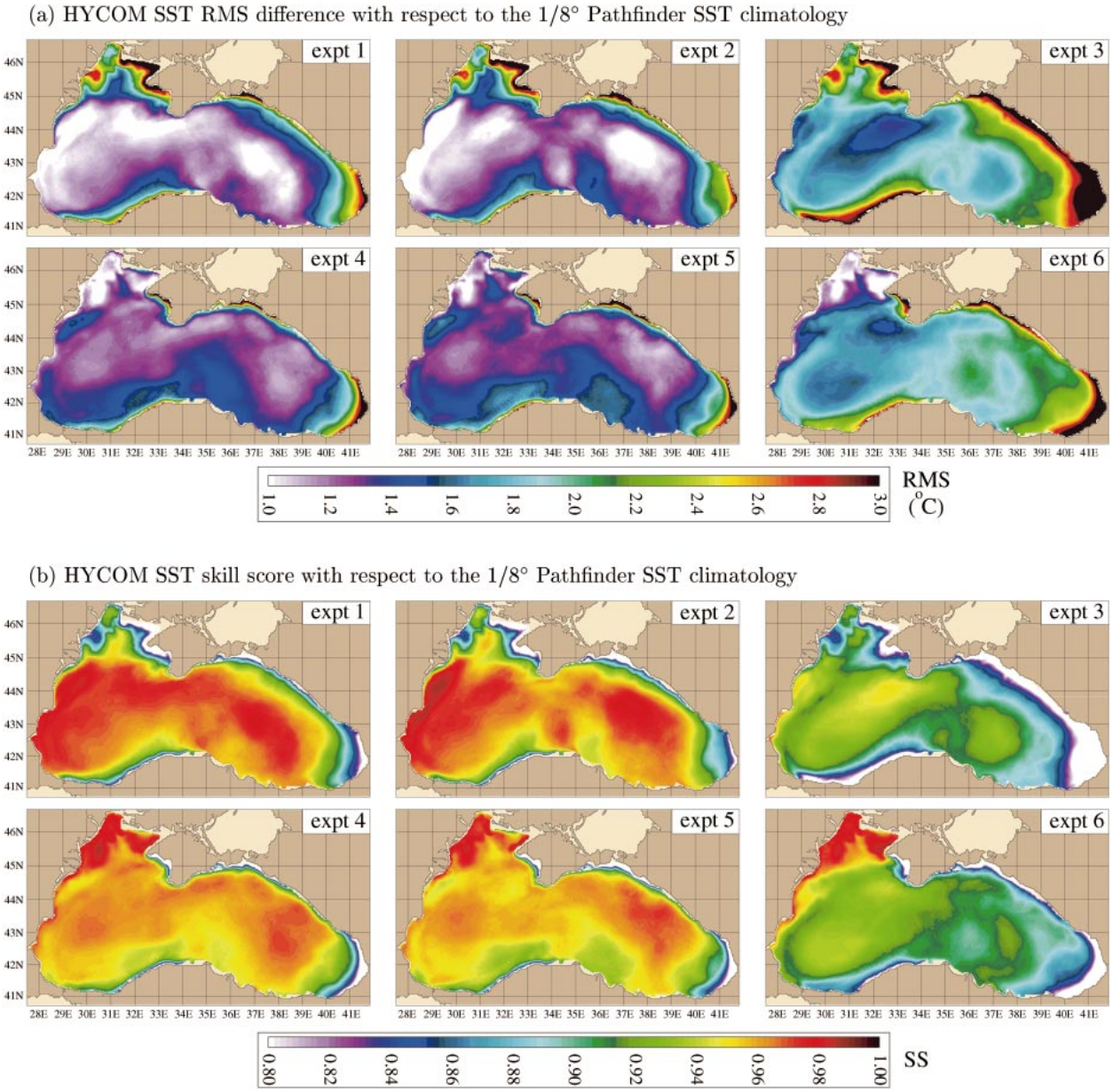

FIG. 8. Maps of statistical comparison between monthly HYCOM SST and the monthly mean Pathfinder SST climatology: (a) rms and (b) SS. Note that expts 1, 2, and 3 are forced with ECMWF wind/thermal fluxes, and expts 4, 5, and 6 are forced with NOGAPS wind/thermal fluxes. In these comparisons the Pathfinder SST climatology is treated as ''perfect.'' Thus, HYCOM can never be more accurate than the Pathfinder SST climatology. An SS value of 1.0 indicates perfect SST predictions from HYCOM. The basin-averaged rms and SS values are given in Table 3 for each experiment.

closer to the experiments that assume all radiation absorbed at the surface (expts 2 and 5, respectively) because of its high turbidity, but there are also relatively large differences between the two, especially in June. Thus, a Black Sea OGCM will need to use space–time varying turbidity.

c. Limitations in the atmospheric forcing

The grid resolution from the two atmospheric forcing products (1.125° × 1.125° for ECMWF and 1.0° × 1.0° for NOGAPS) is much coarser than the HYCOM grid resolution used here ($\frac{1}{25}° \times \frac{1}{32}°$), and some atmospheric surface forcing fields are strongly influenced by land and sea. Thus, the land–sea mask used by these products is important, especially for regions close to the coast in the Black Sea. As discussed in section 4b, the SST errors from the standard HYCOM simulations (expts 1 and 4) tend to be largest in comparison with the Pathfinder climatology in the Black Sea coastal regions, especially with ECMWF forcing along the northern boundary and

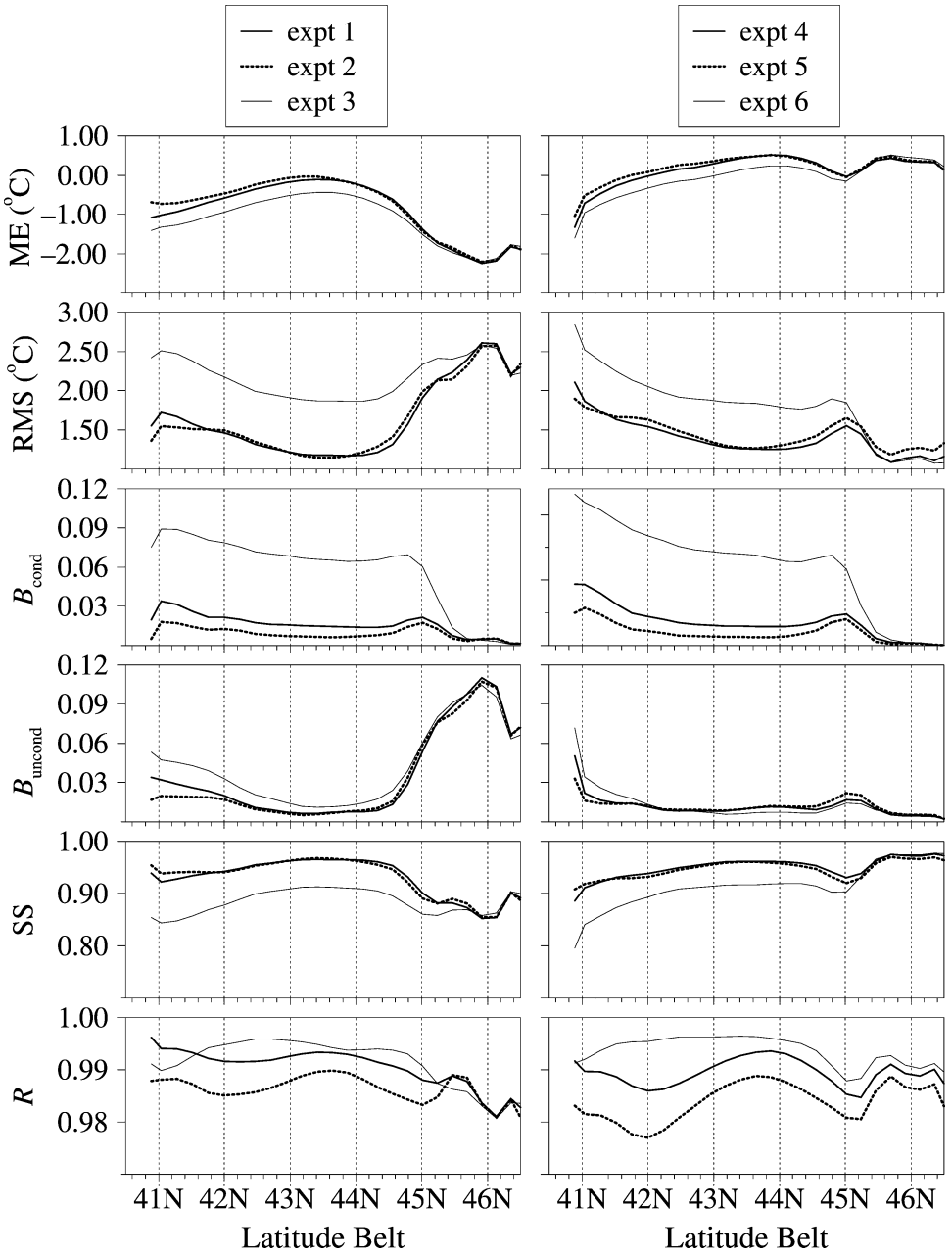

FIG. 9. Zonal averages of statistical metrics comparing monthly mean SST between the 9-km Pathfinder climatology and HYCOM at each model grid point over the Black Sea. Statistics are defined in section 4a. Results are shown for expt 1 (thick solid line), expt 2 (dotted line), and expt 3 (solid line) when the model was forced with ECMWF wind/thermal fluxes; similarly expt 4 (thick solid line), expt 5 (dotted line), and expt 6 (solid line) when the model was forced with NOGAPS wind/thermal fluxes.

over the northwestern shelf. Here, we investigate the possibility that these errors can be largely attributed to the misrepresentation of ocean points in the forcing products.

The land–sea masks used in the original ECMWF reanalysis and NOGAPS products interpolated onto the HYCOM domain are shown in Fig. 10. All grids south of 42.0°N are represented as land points in the ECMWF land–sea mask but most of them should be ocean. There is only one sea grid point east of 39°E in the north–south direction, but there should be two–three grid points, in reality. This means that ECMWF treats some sea points as land points in the Black Sea region. The NOGAPS mask provides a better representation of the

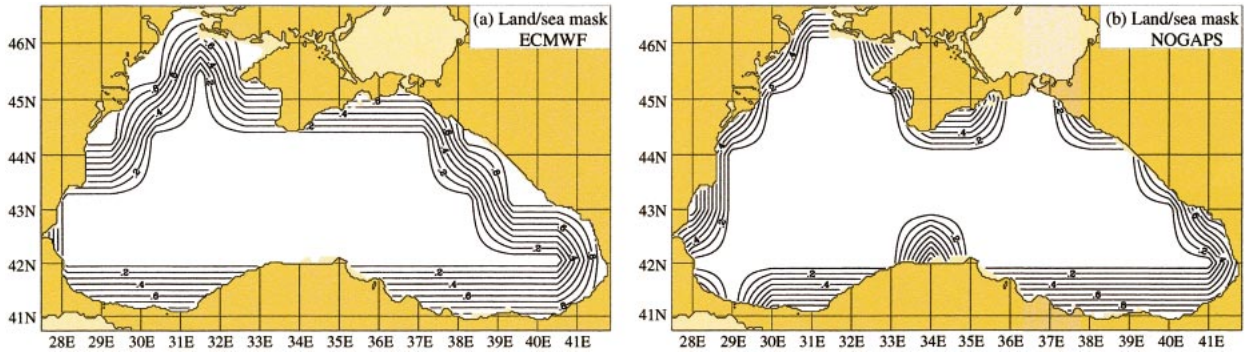

FIG. 10. The land–sea mask for the Black Sea used in (a) the ERA product (1979–93), and (b) the NOGAPS product (1998–2002). The original land–sea mask files are binary; i.e., a grid point is either land (1) or sea (0). We interpolated them from the 1.125° × 1.125° reduced Gaussian grid for ECMWF and 1.0° × 1.0° for NOGAPS to the model grid. In (a) and (b), for example, a contour value of 0.8 implies that the flux values on the model grid were ~80% contaminated by the land flux values. In the northwestern part of the Black Sea the ECMWF land–sea mask, which favors the atmosphere, spreads farther into the Black Sea than does the NOGAPS land–sea mask.

land/sea distribution, but is still limited by its 1.0° × 1.0° resolution. The fact that NOGAPS forcing shows more skill near the coast, despite generally lower skill elsewhere, suggests that SST errors close to the coast, especially over the northwestern shelf, in the easternmost Black Sea, and along the northeast coast, are primarily caused by the incorrect land–sea mask and not by HYCOM itself.

A comparison of Figs. 8 and 10 yields another particularly significant result. The NOGAPS-forced simulations show that HYCOM can simulate accurate SSTs in shallow water, that is, over the broad northwestern shelf. If we had only used ECMWF forcing with the erroneous land–sea mask, we would not have obtained that significant piece of information from this study and might have erroneously concluded that HYCOM does not produce accurate SST in shallow water.

5. Flux and SST relationship

To further investigate sensitivity of HYCOM SST simulations to water turbidity, a possible relationship between heat fluxes and SST is sought. Our major goals are 1) to determine if changes in heat fluxes cause systematic biases in SST and if there are systematic biases and then 2) to find out the statistical relationship between the SST biases and heat flux biases.

For this purpose, the net penetrative heat flux at the surface (Fig. 3) is divided into the penetrating heat flux absorbed within the mixed layer (the mixed layer flux) and the heat flux that penetrates below the mixed layer (sub-mixed-layer heat flux). Then, monthly mean SST differences (Table 4) and sub-mixed-layer heat flux differences between two simulations (e.g., expt 3 − expt 1) are calculated and plotted together over the seasonal cycle. The results in Fig. 11 satisfy the first goal above because changes in the sub-mixed-layer heat flux differences are inversely proportional to changes in the SST differences in all four cases. In particular, the sub-mixed-layer heat flux deviations from the standard simulations using turbidity from SeaWiFS (expts 1 and 4) are strongly related to the corresponding SST differences whether using a clear-water constant attenuation depth of 16.7 m (expts 3 and 6) or assuming all radiation absorbed at the sea surface (expts 2 and 4). Furthermore, the result is independent of the atmospheric forcing product chosen, ECMWF or NOGAPS.

We now seek a possible linear relationship (as suggested by Fig. 11) between the SST differences and heat flux differences to attain the second goal. While it is clear that HYCOM SST is determined by various dynamical factors, the major focus here is only changes in sub-mixed-layer heat fluxes and their possible effects on SST. Thus, it is assumed that SST differences are mainly controlled by sub-mixed-layer heat flux differences between the experiment pairs (e.g., between expt 1 and expt 3). This means, for simplicity, it is assumed that SST difference is only a function of the heat flux difference. A scatter diagram (Fig. 12) indicates that SST differences are linearly correlated to heat flux differences with very large R values of 0.97 for both experiment 3 − experiment 1 and experiment 6 − experiment 4. These R values are statistically significant in comparison to a R value of 0.7 at a 95% confidence interval.

The least squares lines for experiment 3 − experiment 1 and experiment 6 − experiment 4 have slope values of -0.065°C (W m^{-2})$^{-1}$ and -0.058°C (W m^{-2})$^{-1}$, respectively. Based on the slope values, for example, a flux difference of 30 W m^{-2} between experiments 3 and 1 results in an SST difference of -1.9°C between the two. Similarly, a 50 W m^{-2} flux difference causes an SST difference that can be as large as -3.3°C between experiments 3 and 1. Thus, the assumption of clear water over the entire Black Sea yields very unrealistic SST from the model (expt 3) in comparison to the standard simulation (expt 1). The same analogy can also be made between experiments 6 and 4. Given that the slope value is -0.058°C (W m^{-2})$^{-1}$ between experiments 6 and 4,

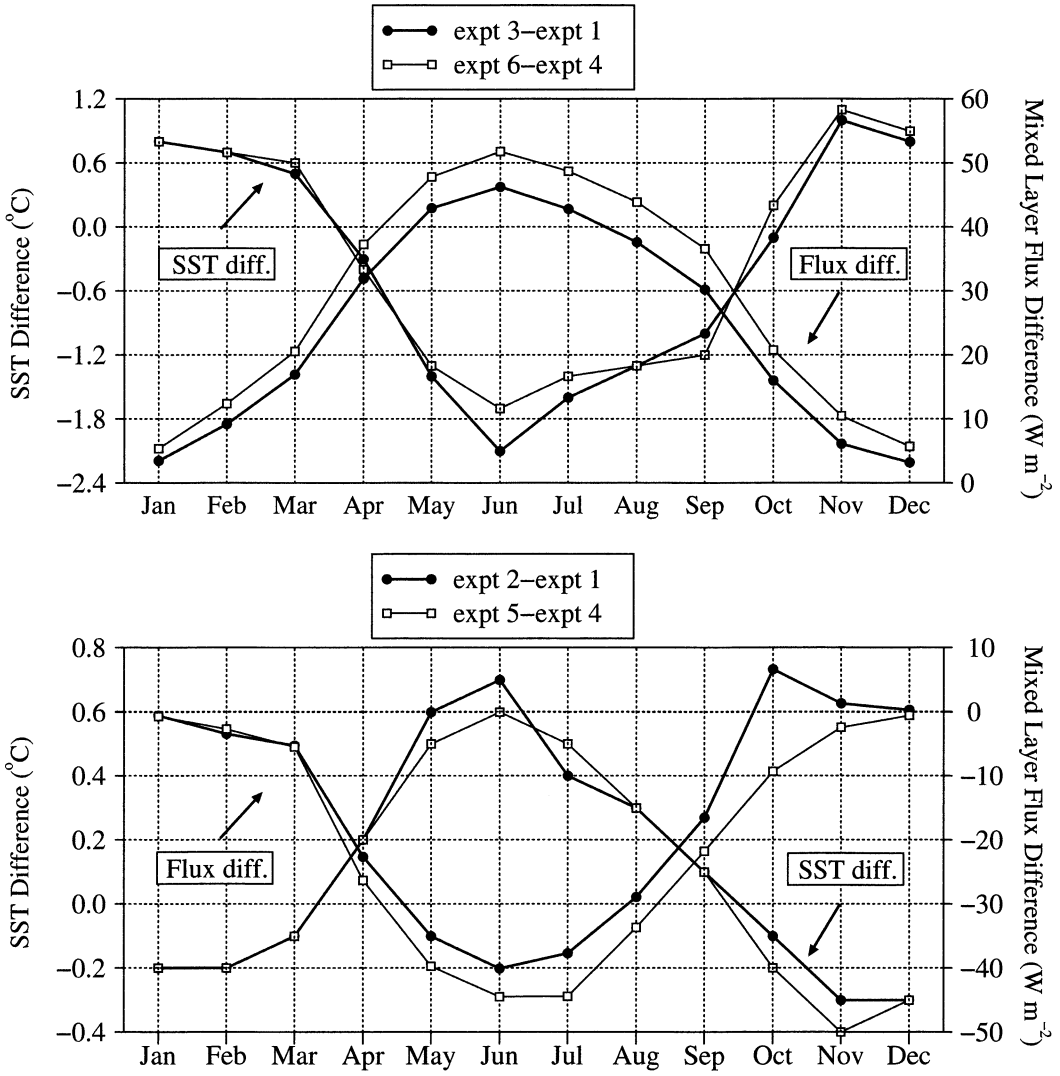

FIG. 11. Monthly mean SST difference and sub-mixed-layer heat flux difference (i.e., difference in shortwave radiation absorbed below the mixed layer). (top) Differences between the clear-water constant attenuation depth simulations (expts 3 and 6) and standard simulations that use spatial and temporal attenuation depths (expts 1 and 4). (bottom) Differences between the simulations that assume all radiation absorbed at the sea surface (expts 2 and 5) and the standard simulations. Note that the *y* axis on the left gives the SST differences and the one on the right gives the flux differences.

heat flux differences of 30 and 50 W m^{-2} result in SST differences of approximately −1.7 and −2.9°C between the two, respectively.

A similar investigation is also made to see whether or not there is any linear relationship between the simulations that assume all radiation absorbed at the sea surface (expts 2 and 5) and standard simulations (expts 1 and 4). Linear relationships are again quite remarkable as evident from statistically significant R values of 0.95 and 0.98 for experiment 2 − experiment 1 and experiment 5 − experiment 4, respectively (Fig. 13). The slopes for experiment 2 − experiment 1 and experiment 5 − experiment 4 are almost equal to each other with values of −0.020°C (W m^{-2})$^{-1}$ and −0.019°C (W m^{-2})$^{-1}$. Thus, a flux difference of, for example, 50 W m^{-2} between experiments 2 and 1 (or between expt 5 and expt 4) gives a SST difference of −1.0°C. Last, it must be emphasized that there are indeed changes in SST in the HYCOM simulations that assume all radiation absorbed at the sea surface as opposed to those which use spatial and temporal monthly mean attenuation depths.

6. Summary and conclusions

Ocean general circulation models play an important role in representing the ocean component of the climate system on a wide variety of temporal and spatial scales.

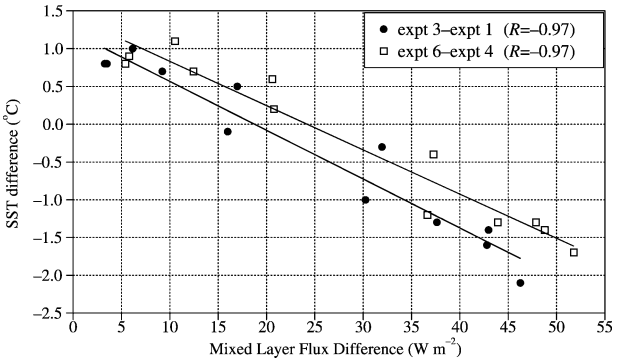

FIG. 12. A scatter diagram of sub-mixed-layer flux differences vs SST differences between the simulations that use a clear-water constant attenuation depth of 16.7 m (expts 3 and 6) and the standard simulations that use spatial and temporal attenuation depths (expts 1 and 4). This figure contains scatterplots of the SST and mixed layer flux difference values that are plotted by month in Fig. 11. Also given in the figure are least squares lines for expt 3 − expt 1 (dark solid line) and for expt 6 − expt 4 (thin solid line). Linear correlation coefficient (R) is given in the upper-right corner for each case. Slope values are -0.065°C (W m^{-2})$^{-1}$ and -0.058°C (W m^{-2})$^{-1}$ for expt 3 − expt 1 and expt 6 − expt 4, respectively.

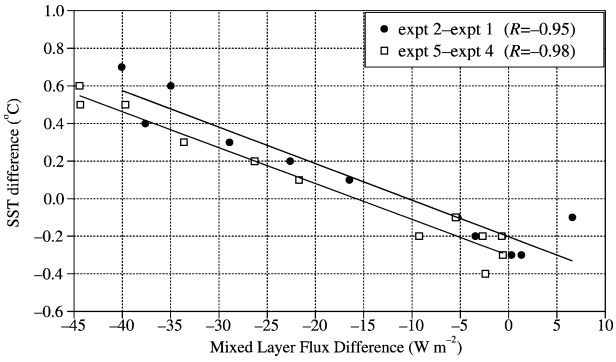

FIG. 13. A scatter diagram of mixed layer flux differences vs SST differences between the simulations that assume all radiation absorbed at the sea surface (expts 2 and 5) and the standard simulations, which use spatial and temporal attenuation depths (expts 1 and 4). Also given in the figure are least squares lines for expt 2 − expt 1 (dark solid line) and for expt 5 − expt 4 (thin solid line). Linear correlation coefficient (R) is given in the upper-right corner for each case. Slope values are -0.020°C (W m^{-2})$^{-1}$ and -0.019°C (W m^{-2})$^{-1}$ for expt 3 − expt 1 and expt 6 − expt 4, respectively.

This paper demonstrates that a fine-resolution (~3.2 km) eddy-resolving Hybrid Coordinate Ocean Model is particularly useful for simulating sea surface temperature (SST) and examining SST sensitivity to water turbidity in the Black Sea. This model combines the advantages of the isopycnal, σ, and z-level coordinates in choosing the optimal coordinate to simulate coastal and open-ocean circulation features, a capability that did not exist in previous Black Sea OGCM studies. The optimal coordinate is chosen dynamically in space and time using the layered continuity equation. The implementation of the KPP mixed layer submodel in HYCOM has a two-band solar radiation penetration scheme that uses a monthly diffusive attenuation coefficient of photosynthetically active radiation (k_{PAR}) climatology based on the SeaWiFs data to account for water turbidity.

In the HYCOM simulations, the basic methodology is to force the model with monthly climatological atmospheric fields (i.e., wind and thermal forcing) from two products (ECMWF and NOGAPS), but with the addition of representative 6-hourly wind stress anomalies. The model SST and accurate bulk formulas in the calculation of latent and sensible heat fluxes. A longwave radiation correction is used in the model simulations to account for the difference between model SST and SST used in the atmospheric forcing product. Based on analysis presented in this paper, a constant value of -5.3 W m^{-2} °C^{-1} is a reasonable approximation ($\pm$20%) to the generally small blackbody radiation correction. This approach is also applicable to other OGCMs.

Model simulations are performed to examine effects of water turbidity in predicting SST. For a quantitative evaluation of the model performance, several statistical measures, such as mean error, root-mean-square difference, correlation coefficient, and skill score are used. Time series of monthly mean SST from HYCOM are then compared with those from a satellite-based climatological field (~9 km Pathfinder SST climatology) at each model grid point over the Black Sea. Climatological error statistics from standard HYCOM simulations, which use spatial and temporal attenuation depths, give a basin-averaged ME of approximately -0.5°C with ECMWF forcing and ~0.2°C with NOGAPS forcing. Both forcing products yield an rms difference of ~1.4°C for the seasonal cycle of SST. Similarly, basin-averaged R and SS values are ~0.99 and ~0.95, respectively. Given that the SST standard deviation is very large (usually $>$ 6°C) in the Black Sea over the annual cycle, having a very large SS value close to 1 demonstrates HYCOM success in predicting monthly mean SST.

While allowing k_{PAR} to vary in time and space is desirable for predicting SST in the Black Sea, absorption of all radiation at the sea surface or using a constant basin-averaged climatological mean k_{PAR} value of 0.19 m^{-1} from the SeaWiFS data also yields comparable results on longer time scales (i.e., annual mean) but not on shorter time scales (i.e., monthly mean) because there is a large seasonal cycle in solar attenuation coefficient. In contrast, using the clear-water constant attenuation depth assumption of $k_{\mathrm{PAR}} = 0.06$ m^{-1} (i.e., $k_{\mathrm{PAR}}^{-1} \approx 16.7$ m) as opposed to using monthly varying water type results in the worst SST simulation from HYCOM. In this case, the basin-averaged SST bias values in relation to the corresponding simulation using SeaWiFS-based turbidity are as large as 2°–3°C in the summer. This large bias is due mainly to differences in the amount of heat flux below the mixed layer in the two cases. In particular, the simulation that assumes clear-water constant attenuation depth over the Black Sea has larger sub-mixed-layer heat

fluxes than the standard simulation using spatially and temporally varying attenuation depths. In the latter, the attenuation depths are much smaller than 16.7 m (typically 5 m). The combination of relatively small attenuation depths and shallow mixed layer depths (typically 3 m) is the main reason for the large flux and SST differences between these simulations in summer. It is also found that SST differences and sub-mixed-layer heat flux differences between these two simulations are linearly correlated on seasonal climatological time scales.

The ability of HYCOM to predict SST in some regions may be limited by the atmospheric forcing product, ECMWF and NOGAPS. Some of the model errors near coastal regions (especially on the broad northwestern shelf, along the northeastern boundary and in the easternmost Black Sea) are clearly due to the land–sea mask used and the relatively coarse resolution of atmospheric forcing products. One particularly significant result is that HYCOM can simulate accurate SST in shallow water (as well as deep) when an accurate land–sea mask is used in the atmospheric forcing product. This was demonstrated over the broad northwestern shelf by the NOGAPS-forced simulation. In contrast, the ECMWF-forced simulation exhibited large SST errors in this region because of an inaccurate land/sea mask. Results presented in this paper confirm accuracy of HYCOM. The model simulation will be extended on interannual time scales, which is the subject of another paper.

Acknowledgments. We extend our special thanks to E. J. Metzger and P. Posey of the Naval Research Laboratory (NRL) at the Stennis Space Center for their suggestions regarding atmospheric forcing fields. Appreciation is extended to R. Bleck of the Los Alamos National Laboratory (LANL) and E. Chassignet and G. Halliwell of the Rosenstiel School of Marine and Atmospheric Science (RSMAS) at the University of Miami for their discusions during the HYCOM development. We thank P. Kållberg of the European Centre for Medium-Range Weather Forecasts (ECMWF) for his comments regarding the ECMWF land/sea mask. The ocean color data used in this paper were obtained from the Goddard Distributed Active Archive Center under the auspices of the National Aeronautics and Space Administration (NASA). Use of these data is in accord with the Sea-Viewing Wide Field-of-View Sensor (SeaWiFS) Research Data Use Terms and Conditions Agreement. The model simulations were performed under the Department of Defense High Performance Computing Modernization Program on an IBM SP POWER3 at the Naval Oceanographic Office, Stennis Space Center, Mississippi, and on an HP/COMPAQ SC45 at the U.S. Army Engineer Research and Development Center (ERDC), Vicksburg, Mississippi. This work is a contribution of the NOPP HYCOM consortium for data-assimilative ocean modeling, and the 6.1 Thermodynamic and Topographic Forcing of Global Ocean Models project. Both are funded by the Office of Naval Research (ONR) under Program Elements 602435N for 6.2 and 601153N for 6.1 projects.

REFERENCES

Beckers, J.-M., 1991: Application of a 3D model to the western Mediterranean. *J. Mar. Syst.,* **1,** 315–332.

——, M. Grégoire, J. C. J. Nihoul, E. V. Stanev, J. Staneva, and C. Lancelot, 2002: Modelling the Danube-influenced shelf of the Black Sea. I: Hydrodynamical processes simulated by 3-D and box models. *Est. Coastal Shelf Sci.,* **54,** 453–472.

Bleck, R., 2002: An oceanic general circulation model framed in hybrid isopycnic-Cartesian coordinates. *Ocean Modell.,* **4,** 55–88.

Blumberg, A. F., and G. L. Mellor, 1987: A description of a three-dimensional coastal ocean circulation model. *Three-Dimensional Coastal Ocean Models*, N. S. Heaps, Ed., Coastal and Estuarine Series, Vol. 4, Amer. Geophys. Union, 1–16.

Bryan, K., 1969: A numerical method for the study of the circulation of the World Ocean. *J. Comput. Phys.,* **3,** 347–378.

Casey, K. S., and P. Cornillon, 1999: A comparison of satellite and in situ based sea surface temperature climatologies. *J. Climate,* **12,** 1848–1863.

da Silva, A. M., C. C. Young, and S. Levitus, 1994: *Algorithms and Procedures.* Vol. 1, *Atlas of Surface Marine Data,* NOAA Atlas NESDIS 6, 83 pp.

Dietrich, D. E., 1997: Application of a modified ''a'' grid ocean model having reduced numerical dispersion to the Gulf of Mexico circulation. *Dyn. Atmos. Oceans,* **27,** 201–217.

Fox, D. N., W. J. Teague, C. N. Barron, M. R. Carnes, and C. M. Lee, 2002: The Modular Ocean Data Assimilation System (MODAS). *J. Atmos. Oceanic Technol.,* **19,** 240–252.

Gibson, J. K., P. Kållberg, S. Uppala, A. Hernandez, A. Nomura, and E. Serrano, 1997: ERA description. ECMWF Re-Analysis Project Report Series 1, 72 pp. [Available from ECMWF, Shinfield Park, Reading RG2 9AX, United Kingdom.]

Grégoire, M., and G. Lacroix, 2001: Study of the oxygen budget of the Black Sea waters using a 3D coupled hydrodynamical–biogeochemical model. *J. Mar. Syst.,* **31,** 175–202.

——, J. M. Beckers, J. C. J. Nihoul, and E. Stanev, 1998: Reconnaissance of the main Black Sea's ecohydro-dynamics by means of a 3D interdisciplinary model. *J. Mar. Syst.,* **16,** 85–106.

Guieu, C., and J. M. Martin, 2002: The level and fate of metals in the Danube River plume. *Est. Coastal Shelf Sci.,* **54,** 439–451.

Gupta, S. K., W. L. Darnell, and A. C. Wilber, 1992: A parameterization for longwave radiation from satellite data: Recent improvements. *J. Appl. Meteor.,* **31,** 1361–1367.

Halliwell, M. R., Jr., 2004: Evaluation of vertical coordinate and vertical mixing algorithms in the Hybrid Coordinate Ocean Model (HYCOM). *Ocean Modell.,* **7,** 285–322.

Jerlov, N. G., 1976: *Marine Optics.* Elsevier Oceanic Series, Vol. 14, Elsevier, 231 pp.

Josey, S. A., R. W. Pascal, P. K. Taylor, and M. J. Yelland, 2003: A new formula for determining the atmospheric longwave flux at the ocean surface at mid-high latitudes. *J. Geophys. Res.,* **108,** 3108, doi:10.1029/2002JC001418.

Kara, A. B., P. A. Rochford, and H. E. Hurlburt, 2000: An optimal definition for ocean mixed layer depth. *J. Geophys. Res.,* **105,** 16 803–16 821.

——, ——, and ——, 2002: Air–sea flux estimates and the 1997–1998 ENSO event. *Bound.-Layer Meteor.,* **103,** 439–458.

——, ——, and ——, 2003: Mixed layer depth variability over the global ocean. *J. Geophys. Res.,* **108,** 3079, doi:10.1029/2000JC000736.

——, H. E. Hurlburt, P. A. Rochford, and J. J. O'Brien, 2004: The impact of water turbidity on the interannual sea surface temperature simulations in a layered global ocean model. *J. Phys. Oceanogr.,* **34,** 345–359.

——, A. J. Wallcraft, and H. E. Hurlburt, 2005a: A new solar radiation penetration scheme for use in ocean mixed layer studies: An application to the Black Sea using a fine-resolution Hybrid Coordinate Ocean Model (HYCOM). *J. Phys. Oceanogr.,* **35,** 13–32.

——, ——, and ——, 2005b: How does solar attenuation depth affect the ocean mixed layer? Water turbidity and atmospheric forcing impacts on the simulation of seasonal mixed layer variability in the turbid Black Sea. *J. Climate,* **18,** 389–409.

Konovalov, S. K., and J. W. Murray, 2001: Variations in the chemistry of the Black Sea on a time scale of decades (1960–1995). *J. Mar. Syst.,* **31,** 217–243.

Korotaev, G. K., O. A. Saenko, and C. J. Koblinsky, 2001: Satellite altimeter observations of the Black Sea. *J. Geophys. Res.,* **106,** 917–933.

Kourafalou, V. H., and E. V. Stanev, 2001: Modeling the impact of atmospheric and terrestrial inputs on the Black Sea coastal dynamics. *Ann. Geophys.,* **19,** 245–256.

Lalli, C. M., and T. R. Parsons, 1997: *Biological Oceanography: An Introduction.* Butterworth-Heinemann, 314 pp.

Large, W. G., J. C. McWilliams, and S. C. Doney, 1994: Oceanic vertical mixing: A review and a model with a nonlocal boundary layer parameterization. *Rev. Geophys.,* **32,** 363–403.

——, G. Danabasoglu, S. C. Doney, and J. C. McWilliams, 1997: Sensitivity to surface forcing and boundary layer mixing in a global ocean model: Annual mean climatology. *J. Phys. Oceanogr.,* **27,** 2418–2447.

Levitus, S., and T. P. Boyer, 1994: *Temperature*. Vol. 4, *World Ocean Atlas 1994,* NOAA Atlas NESDIS 4, 117 pp.

Liu, W. T., A. Zhang, and J. K. B. Bishop, 1994: Evaporation and solar irradiance as regulators of sea surface temperature in annual and interannual changes. *J. Geophys. Res.,* **99,** 12 623–12 637.

Mee, L. D., 1992: The Black Sea in crisis: A need for concerted international action. *Ambio,* **21,** 278–286.

Mellor, G. L., and T. Yamada, 1982: Development of a turbulence closure model for geophysical fluid problems. *Rev. Geophys.,* **20,** 851–875.

Morel, A., and S. Maritorena, 2001: Bio–optical properties of oceanic waters: A reappraisal. *J. Geophys. Res.,* **106,** 7163–7180.

Murphy, A. H., 1988: Skill scores based on the mean square error and their relationships to the correlation coefficient. *Mon. Wea. Rev.,* **116,** 2417–2424.

——, 1992: Climatology, persistence, and their linear combination as standards of reference in skill scores. *Wea. Forecasting,* **7,** 692–698.

——, and H. Daan, 1985: Forecast evaluation. *Probability, Statistics, and Decision Making in the Atmospheric Sciences,* A. H. Murphy and R. W. Katz, Eds., Westview Press, 379–437.

Murtugudde, R., J. Beauchamp, C. R. McClain, M. R. Lewis, and A. J. Busalacchi, 2002: Effects of penetrative radiation on the upper tropical ocean circulation. *J. Climate,* **15,** 470–486.

Nakamoto, S., P. Kumar, J.-M. Oberhuber, J. Ishizaka, K. Muneyama, and R. Frouin, 2001: Response of the equatorial Pacific to chlorophyll pigment in a mixed layer isopycnal ocean general circulation model. *Geophys. Res. Lett.,* **28,** 2021–2024.

Neter, J., W. Wasserman, and G. A. Whitmore, 1988: *Applied Statistics.* Allyn and Bacon, 1006 pp.

Nihoul, J. C. J., E. Deleersnijder, and S. Djenidi, 1989: Modeling the general circulation of shelf seas by 3D k–ϵ models. *Earth Sci. Rev.,* **26,** 163–189.

Oguz, T., and P. Malanotte-Rizzoli, 1996: Seasonal variability of wind and thermohaline driven circulation in the Black Sea: Modeling studies. *J. Geophys. Res.,* **101,** 16 551–16 569.

——, ——, and D. Aubrey, 1995: Wind and thermohaline circulation of the Black Sea driven by yearly mean climatological forcing. *J. Geophys. Res.,* **100,** 6845–6863.

——, H. W. Ducklow, J. E. Purcell, and P. Malanotte-Rizzoli, 2001: Modeling the response of top-down control exerted by gelatinous carnivores on the Black Sea pelagic food web. *J. Geophys. Res.,* **106,** 4543–4564.

——, P. Malanotte-Rizzoli, H. W. Ducklow, and J. W. Murray, 2002: Interdisciplinary studies integrating the Black Sea biogeochemistry and circulation dynamics. *Oceanography,* **15,** 4–11.

Rachev, N. H., and E. V. Stanev, 1997: Eddy processes in semi-enclosed seas. A case study for the Black Sea. *J. Phys. Oceanogr.,* **27,** 1581–1601.

Rayner, N. A., E. B. Horton, D. E. Parker, C. K. Folland, and R. B. Hackett, 1996: Version 2.2 of the Global Sea-Ice and Sea Surface Temperature data set, 1903–1994. Climate Research Tech. Note 74, 42 pp.

Reynolds, R. W., N. A. Rayner, T. M. Smith, and D. C. Stokes, 2002: An improved in-situ and satellite SST analysis for climate. *J. Climate,* **15,** 1609–1625.

Rochford, P. A., A. B. Kara, A. J. Wallcraft, and R. A. Arnone, 2001: Importance of solar subsurface heating in ocean general circulation models. *J. Geophys. Res.,* **106,** 30 923–30 938.

Rosmond, T. E., J. Teixeira, M. Peng, T. F. Hogan, and R. Pauley, 2002: Navy Operational Global Atmospheric Prediction System (NOGAPS): Forcing for ocean models. *Oceanography,* **15,** 99–108.

Schneider, E. K., and Z. Zhu, 1998: Sensitivity of the simulated annual cycle of sea surface temperature in the equatorial Pacific to sunlight penetration. *J. Climate,* **11,** 1933–1950.

Schrum, C., J. Staneva, E. Stanev, and E. Ozsoy, 2001: Air–sea exchange in the Black Sea estimated from atmospheric analysis for the period 1979–1993. *J. Mar. Syst.,* **31,** 3–19.

Smith, T. M., and R. W. Reynolds, 1998: A high-resolution global sea surface temperature climatology for the 1961–90 base period. *J. Climate,* **11,** 3320–3323.

Stanev, E. V., and J.-M. Beckers, 1999: Numerical simulations of seasonal and interannual variability of the Black Sea thermohaline circulation. *J. Mar. Syst.,* **22,** 241–267.

——, and N. H. Rachev, 1999: Numerical study on the planetary Rossby waves in the Black Sea. *J. Mar. Syst.,* **21,** 283–306.

——, and J. V. Staneva, 2000: The impact of the baroclinic eddies and basin oscillations on the transitions between different quasi-stable states of the Black Sea circulation. *J. Mar. Syst.,* **24,** 1–26.

——, and ——, 2001: The sensitivity of the heat exchange at ocean surface to meso and sub-basin scale eddies: Model study for the Black Sea. *Dyn. Atmos. Oceans,* **33,** 163–189.

——, V. M. Roussenov, N. H. Rachev, and J. V. Staneva, 1995: Sea response to atmospheric variability: Model study for the Black Sea. *J. Mar. Syst.,* **6,** 241–267.

Staneva, J. V., and E. V. Stanev, 1998: Oceanic response to atmospheric forcing derived from different climatic data sets. *Ocean. Acta,* **21,** 393–417.

——, K. O. Buesseler, E. V. Stanev, and H. D. Livingston, 1999: The application of radiotracers to a study of Black Sea circulation: Validation of numerical simulations against observed weapons testing and Chernobyl ^{137}Cs data. *J. Geophys. Res.,* **104,** 11 099–11 114.

——, D. E. Dietrich, E. V. Stanev, and M. J. Bowman, 2001: Rim current and coastal eddy mechanisms in an eddy-resolving Black Sea general circulation. *J. Mar. Syst.,* **31,** 137–157.

Sur, H. I., E. Ozsoy, and U. Unluata, 1994: Boundary current instabilities, upwelling, shelf mixing and eutrophication processes in the Black Sea. *Progress in Oceanography,* Vol. 33, Pergamon, 249–302.

——, ——, Y. P. Ilyin, and U. Unluata, 1996: Coastal/deep ocean interactions in the Black Sea and their ecological/environmental impacts. *J. Mar. Syst.,* **7,** 293–320.

Vörösmarty, C. J., K. Sharma, B. M. Fekete, A. H. Copeland, J. Holden, J. Marble, and J. A. Lough, 1997: The storage and aging of continental runoff in large reservoir systems of the world. *Ambio,* **26,** 210–219.

Wallcraft, A. J., A. B. Kara, H. E. Hurlburt, and P. A. Rochford, 2003: The NRL Layered Global Ocean Model (NLOM) with an embedded mixed layer submodel: Formulation and tuning. *J. Atmos. Oceanic Technol.,* **20,** 1601–1615.

Wijsman, J. W. M., P. M. J. Herman, J. J. Middelburg, and K. Soetaert, 2002: A model for early diagenetic processes in sediments of

the continental shelf of the Black Sea. *Est. Coastal Shelf Sci.,* **54,** 403–421.

Yuen, C. W., J. Y. Cherniawsky, C. A. Lin, and L. A. Mysak, 1992: An upper ocean general circulation model for climate studies: Global simulation with seasonal cycle. *Climate Dyn.,* **7,** 1–18.

Zatsepin, A. G., A. I. Ginzburg, A. G. Kostianoy, V. V. Kremenetskiy, V. G. Krivosheya, S. V. Stanichny, and P.-M. Poulain, 2003: Observations of Black Sea mesoscale eddies and associated horizontal mixing. *J. Geophys. Res.,* **108,** 3246, doi:10.1029/2002JC001390.